Strål
säkerhets
myndigheten
Swedish Radiation Safety Authority

Authors: David Savage
             Randy Arthur
             Claire Watson
             James Wilson

Research

2010:12

An Evaluation of Models of Bentonite Pore Water Evolution

This report concerns a study which has been conducted for the Swedish Radiation Safety Authority, SSM. The conclusions and viewpoints presented in the report are those of the author/authors and do not necessarily coincide with those of the SSM.

SSM Perspective

Background
The pore-water composition of a KBS-3 bentonite buffer may gradually change as a result of reaction between groundwater and buffer minerals. The rather minor occurrences of the most rapidly reacting minerals in the buffer will have the most immediate and observable influences, but contributions from slow reactions of the main bulk clay phases cannot be ruled out. The performance implication of such bentonite chemical reaction is that radionuclide solubility and sorption depend on the buffer chemical conditions. Moreover, pore-fluid composition at the interface between the buffer and the surrounding bedrock is important for the modelling and assessment of potential buffer loss scenarios. Any process with the potential to affect this composition needs to be identified and analysed.

Purpose of the Project
The purpose of this project is to assess to smectite hydrolysis as a potential contribution to long-term geochemical processes in a KBS-3 bentonite buffer.

Results
The outcome of this project is a suggested modelling approach for handling the influences of smectite clay transformations in the performance evaluation of a KBS-3 bentonite buffer. In the more traditional buffer geochemical modelling approach, the focus has been on more reactive trace constituents such as calcite, gypsum and pyrite, but the potential bulk-transformation of the main constituent cannot be ignored without justification. In absolute quantitative terms, several uncertainties remain, such as the validity of thermodynamic estimates for smectite properties, the validity of the buffer porosity model, the influence of reaction kinetics and the nature of precipitating new minerals. It is concluded in this study that smectite hydrolysis may (based on model predictions) be significant for the future geochemical state of a buffer, but that the time-scale of smectite hydrolysis is too long for experimental verification. The utilized experimental data could therefore not

determine whether or not the process has performance implications for safety assessment. Potential performance significances of such process are as described above related to buffer pH variations and pore-fluid cation composition.

Future work
The authors suggest that the importance of smectite hydrolysis could be further studied through field observation of natural clay-water systems that have evolved over long time scales. Additional exploratory geochemical or bounding performance calculations could also be envisaged. The groundwater evolutionary pathway at potential repository sites with consideration of other engineering materials such as cement could be analysed with the purpose of determining thermodynamic driving forces for smectite alteration.

Project Information
Project manager: Bo Strömberg
Project reference: SSM 2008
Project number: 200810214 and 20081022

Content

2

Executive Summary

The determination of a bentonite pore water composition and understanding its evolution of with time underpins many radioactive waste disposal issues, such as buffer erosion, canister corrosion, and radionuclide solubility, sorption, and diffusion, *inter alia*.

The usual approach to modelling clay pore fluids is based primarily around assumed chemical equilibrium between Na^+, K^+, Ca^{2+}, and Mg^{2+} aqueous species and ion exchange sites on montmorillonite, but also includes protonation-deprotonation of clay edge surface sites, and dissolution-precipitation of the trace mineral constituents, calcite and gypsum. An essential feature of this modelling approach is that clay hydrolysis reactions (i.e. dissolution of the aluminosilicate octahedral and tetrahedral sheets of montmorillonite) are ignored. A consequence of the omission of clay hydrolysis reactions from bentonite pore fluid models is that montmorillonite is preserved indefinitely in the near-field system, even over million-year timescales.

Here, we investigate the applicability of an alternative clay pore fluid model, one that incorporates clay hydrolysis reactions as an integral component and test it against well-characterised laboratory experimental data, where key geochemical parameters, Eh and pH, have been measured directly in compacted bentonite. Simulations have been conducted using a range of computer codes to test the applicability of this alternative model. Thermodynamic data for MX-80 smectite used in the calculations were estimated using two different methods.

Simulations of 'end-point' pH measurements in batch bentonite-water slurry experiments showed different pH values according to the complexity of the system studied. The most complete system investigated revealed pH values were a strong function of partial pressure of carbon dioxide, with pH increasing with decreasing PCO_2 (log PCO_2 values ranging from -3.5 to -7.5 bars produced pH values ranging from 7.9 to 9.6).

A second set of calculations investigated disequilibrium between clay and pore fluid in laboratory squeezing cell tests involving pure water (pH = 9.0) or a 1M NaOH solution (pH = 12.1). Simulations carried out for 100 days (the same timescale as the experiments) showed that smectite remained far from equilibrium throughout, and that pH decreases due to smectite hydrolysis were trivial. However, extending the duration of the simulations to that required for clay-fluid equilibrium, necessitated timescales of 7 and 65 years for pure water and 1M NaOH, respectively, but again produced relatively minor pH decreases in the order of 0.1-0.2 pH units. If the (equilibrium) precipitation of secondary minerals was included in the simulations, then not only was the clay-fluid equilibration period extended dramatically (from 7 to 360 years for pure water, and from 65 to 2600 years for 1 M NaOH), but concomitant changes in pH were significant, decreasing from 9.0 to 8.6 (pure water) and from 12.1 to 9.0 (1 M NaOH). Repetition of these latter calculations using an alternative method of estimating the ΔG_f^0 of smectite

produced an increase in equilibration time for reaction with 1M NaOH from 2600 to 5000 years, highlighting the potential effects of the uncertainty in thermodynamic data for smectite.

A final set of calculations was carried out to investigate both the time- and space-dependent variations in pore fluid composition in laboratory in-diffusion experiments conducted for over 1200 days, initially with pure water and 'spiked' after 271 days with a Na-Ca-OH-Cl solution (pH = 11.7). Here, the sensitivity of the results to both variations in a number of parameters/conditions (porosity, reaction rate of secondary minerals, the degree of mixing of the external fluid reservoirs in the experiments, the effective diffusion coefficient) and the inclusion/exclusion of key processes (clay hydrolysis, secondary mineral precipitation, ion exchange, clay edge protonation-deprotonation reactions) was investigated. These calculations confirmed that smectite hydrolysis alone has an insignificant impact upon pH buffering over lab timescales and that the pH buffering observed is most likely controlled by clay protonation-deprotonation reactions, and kinetic secondary mineral (brucite + tobermorite) precipitation, using a total porosity model (simulations using a geochemical porosity value produced a poor fit to the experimental data). Ion exchange was not important in controlling pH. The pH of the initial bentonite pore water is ascribed to the presence of trace amounts of CO_2 in the experiments, although calcite played an insignificant role in pH buffering. Alternative data for the kinetic hydrolysis of smectite produced no observable differences, and the adoption of a reduced diffusion coefficient produced a poorer fit to experiment results.

In conclusion, modelling predicts that the effects of smectite dissolution on the chemistry of bentonite pore waters would be essentially undetectable over experimental time scales, but when the model is combined with plausible constraints on the precipitation of secondary phases, significant changes in solution chemistry and mineralogy are predicted to occur over time scales that are relevant to repository near-field evolution (hundreds to thousands of years). There are remaining fundamental uncertainties related to the variable chemistry of the smectite clays, the nature of porosity in highly compacted buffer materials, the reactive surface area of smectite, and the thermodynamic properties of these clay minerals. Studies of natural clay-water systems that have evolved over long periods of time could help provide a new perspective on these uncertainties, and approaches that could be used to help resolve them.

1. Introduction

The determination of a bentonite pore water composition and understanding the evolution of its likely chemical composition with time underpins many other repository near-field activities, such as understanding buffer erosion, canister corrosion, and radionuclide solubility, sorption, and diffusion, *inter alia* and thus plays a vital, if indirect, rôle in safety assessment.

Key parameters in definition of this pore water composition are pH and Eh, which have major effects on canister corrosion and radionuclide solubility and migration, and concentrations (activities) of aqueous species which may accelerate metal corrosion, and/or enhance radionuclide solubilities/mobilities. Species in this category would include HS^-, HCO_3^-, and Cl^-. An important aspect of this evaluation is not only to define a (starting) pore water composition, but also to gain insight into controlling processes and mechanisms, such that changes in pore water composition can be predicted when the system is subject to internal (e.g. waste thermal output) and external (e.g. changing host rock groundwater composition) perturbations.

Redox in bentonite pore fluids is generally assumed to be controlled by chemical equilibria involving dissolved iron species and iron-bearing minerals, such as Fe^{2+}/Fe_3O_4 (e.g. [1]), or alternatively, by $Fe^{2+}/siderite$ (e.g. [2]). Reactions involving reduced sulphur species are deemed of lesser importance because of the assumed non-viability of sulphate-reducing bacteria in compacted bentonite ([2]). To a certain extent, the precise controlling reactions are a site-specific issue, in that the concentrations of redox-sensitive species may be dominated by the composition of the ambient groundwater at a disposal site.

pH is assumed to be determined through the interaction of a number of factors, such as:

- ion exchange on clay;
- protonation-deprotonation reactions at clay edge sites;
- dissolution-precipitation reactions of trace carbonate minerals (calcite, siderite, dolomite);
- dissolution-precipitation reactions of the major clay mineral component (montmorillonite) of the bentonite;
- the concentration of conservative anions (usually Cl^-) in the ambient groundwater;
- and the assumed partial pressure of carbon dioxide (PCO_2) of the system.

Different authors place different emphasis on each of the above factors, but the consensus is that the clay fraction principally acts as a cation exchanger, with the clay silicate exchanger being essentially inert and pH being determined by the contribution from the trace carbonate mineral concentration, and the ambient PCO_2/chloride activity (e.g. [2]; [1]). However, there are question marks concerning the thermodynamic validity of ion exchange-based models for clay (e.g. [3]), and a more rigorous approach employing a

solid-solution model for montmorillonite has been advocated ([4]). Ironically, the corollary of this is that although bentonite is part of the 'engineered' barrier system, to all intents and purposes, adoption of an ion exchange-based model necessitates that pH is fixed by the ambient geochemical conditions (PCO$_2$, [Cl$^-$]) at a repository location, rather than by the essential mineral component (montmorillonite) of the bentonite itself.

A consequence of the omission of clay hydrolysis reactions from pore fluid evolution models is that montmorillonite is preserved indefinitely in the near-field system, even over million-year timescales. However, this is contrary to natural systems evidence where smectite clays may undergo dissolution-precipitation reactions over assessment-relevant timescales at pH 9-10 and temperatures of 50-60 °C (e.g. [5]). It may be concluded therefore that although the current approach may be satisfactory to interpret the results of laboratory or in situ experiments, it is not necessarily sufficient to be extended to the timescales of interest for repository safety assessment.

Here, we propose an alternative clay pore fluid model, one which incorporates clay hydrolysis reactions as an integral component of the model and is tested against suitable well-characterised laboratory experimental data. Researchers at VTT in Finland have reported the results of laboratory experiments which have measured key geochemical parameters, Eh and pH, directly in compacted bentonite ([6]). These measurements have been achieved by using solid-state electrodes in conjunction with standard chemical analysis of squeezed pore fluids for calibration purposes. Experiments have been conducted in diffusion cells, squeezing cells, and batch type apparatus, thus providing both single 'end-point' type results and time- and space-dependent squeezing and in-diffusion results. Data from these experiments provide a means of testing geochemical models for bentonite pore fluid evolution and have provided the focus for the modelling activities described here.

2. Conceptual Models for Clay Pore Fluid Behaviour

Intimately related to any model of the evolution pore fluid composition is the understanding of pore fluid behaviour in compacted bentonite, particularly with regard to the nature of porosity and the behaviour of fluids in close proximity to charged clay surfaces. Currently-available conceptual models for clay-pore fluid behaviour consist of either a system with different porosity types, or a system with a single porosity. Both models are discussed in more detail below.

Many researchers view compacted bentonite as possessing different types of porosity, (e.g. [7]; [8]; [9]; [10]; [11]; [6]; [12]) (Figure 1). In this concept, 'total porosity' refers to the total volume of voidage, without discrimination regarding location or type, whereas 'interlamellar/interlayer porosity' is located in the interlayer spaces of individual clay particles, between the individual tetrahedral-octahedral-tetrahedral (TOT) sheets ([10]). This is considered to be a few monolayers thick and because of its more structured nature, is likely to have different properties from 'free water'. 'External porosity' can be viewed as being of two types: that which consists of water in electrical double layers on the surfaces of the clay particles ('double layer water'); 'free water' ([10]) or 'chloride porosity' ([6]), which consists of water as interconnected thin films on the outside of clay stacks and also as films surrounding other minerals (e.g. quartz) in the bentonite. The amounts of each porosity type are thought to vary with compaction density in bentonite (e.g. [13]), with free/chloride porosity being significantly less than the total porosity as compaction density increases (Figure 2).

In this model, diffusion of cations is envisaged to take place both through the interlamellar porosity and the free porosity, whereas diffusion of chloride and other anions takes place solely though the free porosity (e.g. [12]). At high ionic strengths, diffusion of cations is thought to take place preferentially though the free porosity. This interpretation leads to an effective diffusion coefficient which varies according to ionic strength. A corollary of this conceptual model is that bentonite acts as a semi-permeable membrane at high compaction densities, and is effectively impermeable to ionic species in groundwater external to the bentonite ([9]). However, this is contrary to some experimental evidence where 'external ions' have been shown to be introduced to bentonite at high compaction densities (e.g. [14]).
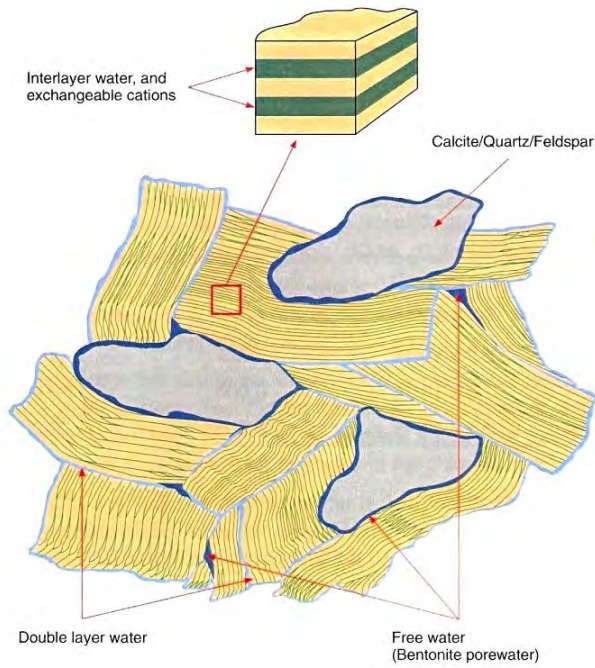
Figure 1. *Schematic diagram of the nature of water in compacted bentonite. From [10].*
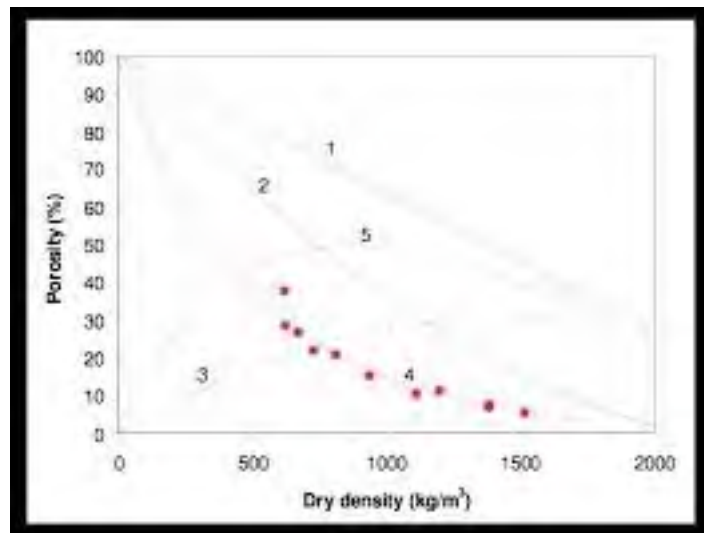

Figure 2. *Different porosity types in compacted bentonite. 1 = total porosity; 2 = external porosity ('double layer' water + 'free' water); 3 = 'interlamellar'/'interlayer' porosity; 4 = 'chloride'/'free' porosity; 5 = porosity inaccessible by chloride. From [13].*

An alternative conceptual model to that described above is offered by Karnland and co-workers ([14]; [15]) which consists of a bentonite-pore fluid system consisting of one porosity type and where pore fluid composition is controlled by ion equilibria within the interlamellar pore space involving two basic processes: Donnan equilibrium which reduces concentrations of external ions compared with external pore fluids; and cation exchange, which affects systems only with more than one type of cation. Consequently, the clay-pore fluid system is envisaged to consist of clay particles acting as macro-ions, and the entire clay-water system may be viewed as a 'polyelectrolyte' (Figure 3).

Birgersson and Karnland ([15]) derive a general expression to describe the effective diffusion coefficient (De) for transport of aqueous species in compacted bentonite:

$$D_e = \phi_c \Xi \frac{\varsigma}{2+\varsigma} D_c \tag{1}$$

where ϕ_c is the total clay porosity; Ξ is a general ion equilibrium coefficient; ς describes the influence of filters (in experimental systems with filters separating fluid reservoirs from the clay), and D_c is the diffusion coefficient in the clay. Normally (for typical filters and sample lengths), the parameter ς is only of importance for cation tracers in very low background concentrations, since the flux of the tracer then will be very high and the filters may be a restriction (O. Karnland, pers. comm.). The ion equilibrium coefficient (Ξ) is a general coefficient in order to express the concentration discontinuities over the solution/bentonite interface. In the case of anions, Ξ represents the Donnan equilibrium effect, whereas in the case of cations, Ξ represents the combined effects of cation exchange and Donnan equilibrium. At low and medium background concentrations, only the ion exchange term is of importance (O. Karnland, pers. comm.). The typical situation for tracer tests in bentonite is that anion concentration will be strongly suppressed in the bentonite, and that cation concentrations will be strongly enhanced.

Birgersson and Karnland ([15]) argue that the acceptance of the existence of only one type of porosity in compacted bentonite obviates the need to describe two separate methods of describing anion and cation diffusion and thus their model brings a greater symmetry to the understanding of transport in compacted bentonite. Thus removing all but one type of pore structure greatly reduces the amount of model parameters to one, the interlayer pore diffusivity (D_c). Furthermore, the single pore type model is not only consistent with, but also allows for calculation of, the swelling pressure under various physicochemical conditions ([16]; [17]).
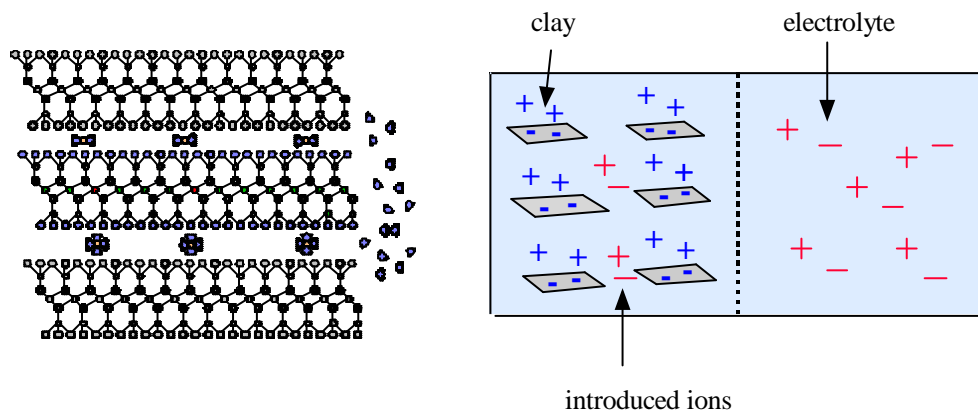
Figure 3. *The single porosity model of the clay-pore fluid system. The clay is seen as a 'soluble polyelectrolyte', contributing positively and negatively charged ions to the clay-water system. An osmotic equilibrium is set up between the clay and external electrolyte, involving diffusion of water molecules and ionic species. From [18].*

The findings of Birgersson and Karnland ([15]) also have large implications for the conceptual view of pore water chemistry. Since in their model, the major part of cations and anions reside in the interlayer pores, this volume is of crucial importance and cannot be ignored in characterising the bentonite pore water chemistry. This approach is thus in sharp contrast to the 'variable porosity' model where pore fluid is considered to reside in the 'free water' porosity only.

3. Experimental Data

VTT in Finland has reported laboratory experimental data concerning the *in situ* measurement of Eh and pH in compacted bentonite ([6]; [19]). It is considered that these data currently constitute the best test of the accuracy of bentonite pore fluid models over short timescales. VTT conducted three basic types of experiments: 'batch'; 'squeezing'; and 'diffusion'. The batch and squeezing experiments were similar in that both resulted in single 'end-point' calculations of pH. The diffusion experiments modelled the evolution of pH (and Eh in some instances) over long timescales (in excess of 1200 days).

Muurinen and Carlsson ([6], [19]) carried out 3 batch experiments in centrifuge tubes. These experiments employed lower bentonite densities than squeezing experiments (below) and fluids were separated at the end of each experiment by centrifugation. Experiment durations were 12 days. Bentonite densities, porosities (total, and what Muurinen and Carlsson ([6], [19]) describe as 'external' and 'chloride' porosities) and pH were all measured/calculated.

Muurinen and Carlsson ([6], [19]) also carried out three experiments in squeezing apparatus. The initial bentonite dry density was about 8 %. These experiments contained approximately 11 g of clay and approximately 9 g of (pure) water. The experiments were conducted for 21 days. Again, bentonite densities, porosities (total, and what Muurinen and Carlsson ([6], [19]) describe as 'external' and 'chloride' porosities) and pH values were measured. The results of all pH measurements in experiments '*L1*' and '*L2*' are shown in Figure 4 and Figure 5, respectively.

Muurinen and Carlsson ([6], [19]) describe an experiment in a cylindrical diffusion cell ('experiment DIF6') in which they monitor pH in compacted bentonite, both before and after, introduction of a high pH, high salinity fluid (Figure 6). In these experiments, bentonite was mixed with deionised water and compacted, before transferral to a diffusion cell. The bentonite sample had a target dry density of 1.5 g cm^{-3}, with a diameter of 40 mm and length of 50 mm. The total porosity was nominally 45.6 % and the geochemical (free) porosity was 6 %. The bentonite remained in contact with an external solution of 10 ml volume via a titanium filter plate. The bentonite sample cell had measurement electrodes at 5, 10, and 20 mm from the contact with the external solution. The apparatus was kept in a nitrogen-filled glovebox for the duration of the experiment. The total duration of the experiment was in excess of 1200 days. The measured *in situ* pH at various depths within the clay sample versus time in the diffusion experiment is presented in Figure 7.
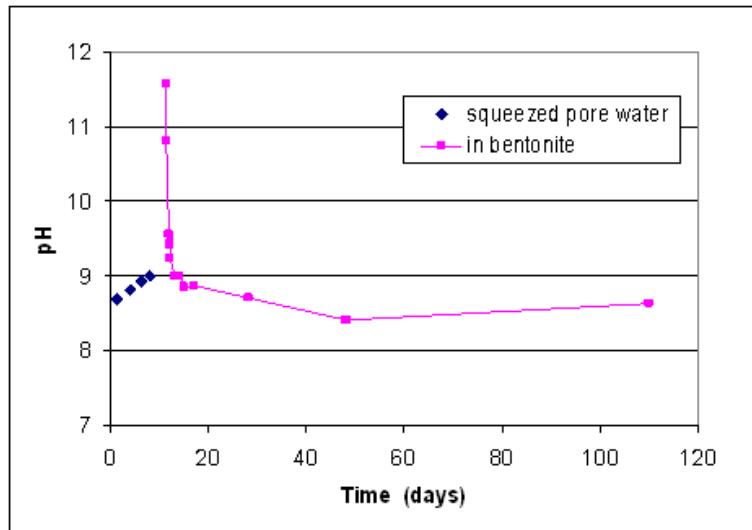
Figure 4. Summary of pH measurements in experiment L1 ([6], [19]). The composition of the final squeezed porewater (pH 9) is shown in Table 8. Initial in-situ measurements using the IrO_x electrode ('in bentonite') are affected by transient disturbances to the bentonite-water system caused by emplacement of the reference electrode ([6], [19]). These disturbances largely dissipate within a day or two.
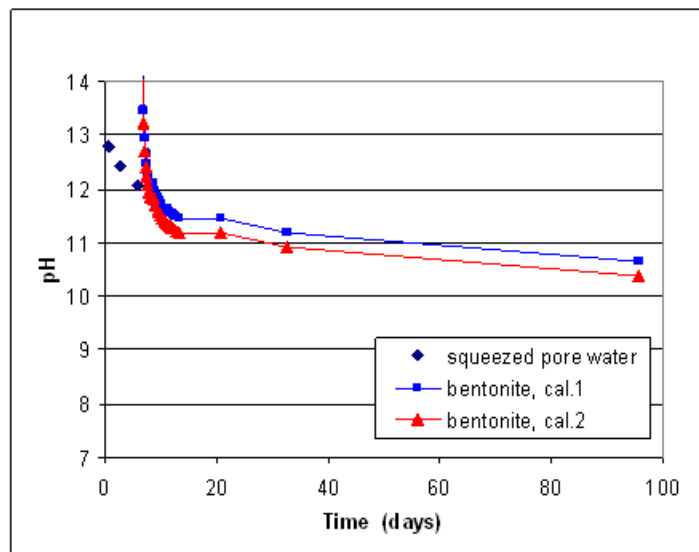

Figure 5. Summary of pH measurements in experiment L2 ([6], [19]). The composition of the final squeezed pore water (pH 12.1) is shown in Table 8. Measurements using the IrO_x electrode are shown for calibrations before ('cal. 1') and after ('cal. 2') the experiment. Initial results are affected by disturbances to the bentonite-water system caused by electrode emplacement.
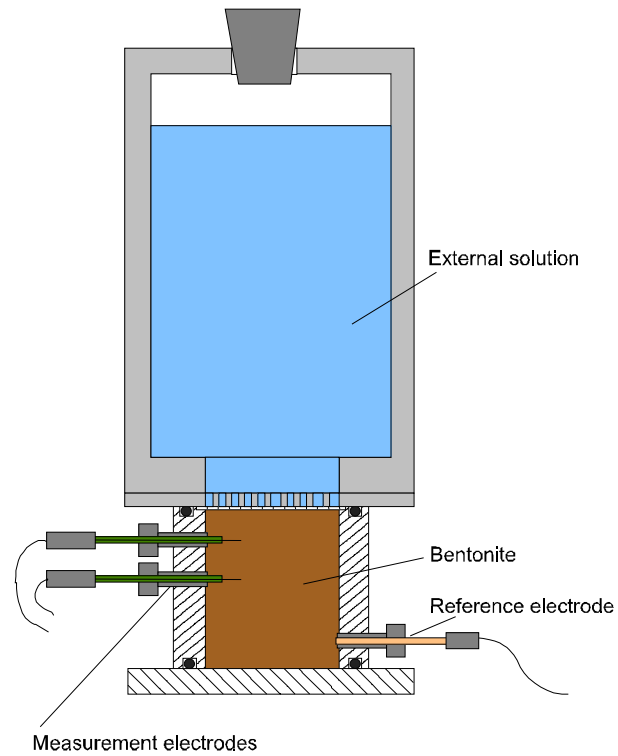
Figure 6. *Schematic diagram of the diffusion cell. From Muurinen and Carlsson ([6], [19]).*
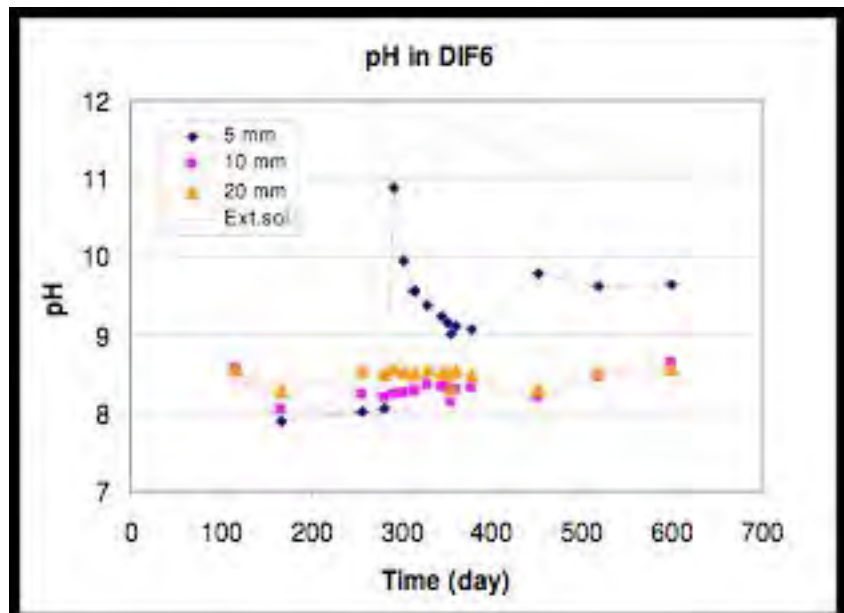

Figure 7. *pH versus time for the diffusion experiment 'DIF6'.   From Muurinen and Carlsson ([6], [19]).*

14

4. Model Input

4.1 Bentonite compositions

The bentonite used in the VTT experiments was MX-80, in 'standard' form, i.e. without any pre-treatment. For their modelling work, Muurinen and Carlsson ([6], [19]) do not define a precise composition of MX-80, and assume that the bentonite consists wholly of clay, with the presence of quartz or calcite 'in excess', i.e. in a large enough proportion to maintain fluids in chemical equilibrium with these minerals. Halite and gypsum are present in trace amounts in the clay which Muurinen and Carlsson ([6], [19]) quote as $1.35 \ 10^{-6}$ mol g^{-1} and $2.35 \ 10^{-5}$ mol g^{-1}, respectively. For the purposes of the modelling work described here, it is necessary to define a specific composition for MX-80. A simplified composition is compared with the measured composition (from [20]) in Table 1. The porosity value in Table 1 is as quoted by Muurinen and Carlsson ([6], [19]) for samples of 1.5 g cm^{-3} density.
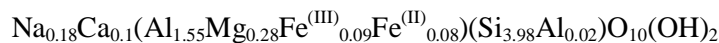
4.2 Ion exchange and surface reactions

Ion exchange constants for montmorillonite derived from [10] (Table 2) were employed, along with a total cation exchange capacity (CEC) for MX-80 of 0.734 mol kg^{-1}, comprising: Na (0.668); K (0.013); Ca (0.033); and Mg (0.02). Regarding clay surface reactions, the data for protonation and deprotonation at two clay edge sites on montmorillonite, S1 and S2 from [10] were used (Table 3).

4.3 Mineral hydrolysis

4.3.1 Smectite

The composition adopted in this study is that reported by [21]:

$$Na_{0.18}Ca_{0.1}(Al_{1.55}Mg_{0.28}Fe^{(III)}_{0.09}Fe^{(II)}_{0.08})(Si_{3.98}Al_{0.02})O_{10}(OH)_2$$

The Gibb's free energy of formation (ΔG^0_f) of this half unit cell formula was estimated using two techniques: that described by Vieillard ([22]); and by the so-called 'Polymer Model' ([23]). A comparison of results obtained using the two estimation techniques can provide some insight concerning uncertainties in the estimated values, and the consequences of such uncertainty on predictions made using kinetic and equilibrium models of smectite-water reactions.

Table 1. *MX-80 composition. From [20], [6], and [19].*

	Measured wt %	Simplified wt %	Simplified vol %
Montmorillonite	87	90	48.7104
Quartz, SiO_2	5	8.5921	4.8666
Feldspar and mica	7	-	-
Calcite, $CaCO_3$	0	1	0.5535
Pyrite	0.07	-	-
Gypsum $CaSO_4{:}2H_2O$	0.7	0.4	0.2603
Halite, NaCl	-	0.0079	0.0055
Porosity	-	-	45.6037

Table 2. *Ion exchange constants for MX-80 bentonite (from [10]).*

Ion exchange reaction	Log K
$ZNa + K^+ = ZK + Na^+$	0.6021
$2ZNa + Ca^{2+} = Z_2Ca + 2Na^+$	0.4150
$2ZNa + Mg^{2+} = Z_2Mg + 2Na^+$	0.3424

Table 3. *Site types, site capacities and protolysis constants for montmorillonite. From [10].*

Site types	Site capacities	Surface complexation reaction	Log K
S^1OH	$4.0\ 10^{-2}$	$S^1OH + H^+ = S^1OH_2^+$	4.5
		$S^1OH = S^1O^- + H^+$	-7.9
S^2OH	$4.0\ 10^{-2}$	$S^2OH + H^+ = S^2OH_2^+$	6.0
		$S^2OH = S^2O^- + H^+$	-10.5

Estimation using the Vieillard model

The Gibb's free energy of formation (ΔG_f^0) of this half unit cell formula was estimated using the method described by Vieillard ([22]):

$$\Delta G_f^0 = \Delta G_{ox}^0 + \sum n_i \Delta G_f^0 (M_i O_{xi}) \tag{2}$$

where ΔG_{ox}^0 is the Gibbs free energy of formation of the mineral of interest from constituent oxides and the second term is the Gibbs free energy of formation of the constituent oxides. Each constituent oxide has a cation (M) present in amount i with associated oxygens in amount x_i and n is the number of moles of M oxide present in the smectite formula. The term ΔG_{ox}^0 is calculated using the expression ([22]):

$$\Delta G_{ox}^0 = -12 \left\{ \sum_{i=1}^{i=ns-1} \sum_{j=i+1}^{j=ns} X_i X_j \left[\Delta_G O = M_i^{Zi} clay - \Delta_G O = M_j^{Zj} clay \right] \right\} \tag{3}$$

where for a given pair of cations in the clay mineral (M_i and M_j), X_i and X_j are the mole fractions of oxygen associated with those cations, $\Delta_G O = M_i^{Zi} clay$ and $\Delta_G O = M_j^{Zj} clay$ are parameters that characterises the electronegativity of cations M_i and M_j (with charge z) and ns refers to the number of different cations and sites. The value of ΔG_{ox}^0 for each mineral of interest is determined by the summation of several interaction terms $\left[\Delta_G O = M_i^{Zi} clay - \Delta_G O = M_j^{Zj} clay \right]$ between pairs of constituent cations (i and j).

Vieillard ([22]) determined values of $\Delta_G O = M^Z clay$ by minimising the difference between calculated ΔG_{ox}^0 values and those derived from reported equilibrium constants for clay mineral solubility. This model ([24]) seems to give more accurate estimates than other models reported in the literature ([22], [24]) (

Table 4). In addition, the model inherently includes a contribution to ΔG_f^0 related to the hydration of interlayer cations, as it is based on measured values.   In order to calculate log K_r values for dissolution reactions (Table 5), values for congruent dissolution of MX-80 smectite were then computed using the estimated smectite ΔG_f^0 value and values for aqueous species which were taken from the SUPCRT92 ([25]) database 'dprons96.dat', which is compatible with the database used in the modelling described here (Table 5). Log K_r values were computed for both the original smectite composition given by [21] and for a simplified composition which does not contain iron. The iron-free composition was used to model the diffusion experiment DIF6.

Table 4. *Summary of thermodynamic data for MX-80 smectite compositions (anhydrous half unit cell compositions) using the Vieillard and Polymer models.*

Smectite Composition	M_r (g mol^{-1})	ΔG_f^o (kJ mol^{-1})	
		Vieillard	Polymer
$Na_{0.18}Ca_{0.1}(Al_{1.55}Mg_{0.28}Fe^{(III)}_{0.09}Fe^{(II)}_{0.08})(Si_{3.98}Al_{0.02})O_{10}(OH)_2$	372.595	-5251.27	-5267.3
$Na_{0.18}Ca_{0.1}(Al_{1.64}Mg_{0.36})(Si_{3.98}Al_{0.02})O_{10}(OH)_2$	367.4740	-5316.28	-

Table 5. Log K values for smectite dissolution reactions using the Vieillard and Polymer models.

Smectite Dissolution Reaction	log K (25°C, 1 bar)	
	Vieillard	Polymer
$Na_{0.18}Ca_{0.1}(Al_{1.55}Mg_{0.28}Fe^{(III)}_{0.09}Fe^{(II)}_{0.08})(Si_{3.98}Al_{0.02})O_{10}(OH)_2$ + 6.08H$^+$ = 0.18 Na$^+$ + 0.1 Ca^{2+} + 1.57 Al^{3+} + 0.28 Mg^{2+} + 0.09 Fe^{3+} + 0.08 Fe^{2+} + 3.98 SiO$_{2(aq)}$ + 4.04 H$_2$O	4.8881	2.07
$Na_{0.18}Ca_{0.1}(Al_{1.64}Mg_{0.36})(Si_{3.98}Al_{0.02})O_{10}(OH)_2$ + 6.08H$^+$ = 0.18 Na$^+$ + 0.1 Ca^{2+} + 1.66 Al^{3+} + 0.36 Mg^{2+} + 3.98 SiO$_{2(aq)}$ + 4.04 H$_2$O	5.9941	-

Estimation using the Polymer model

An alternative technique is referred to as the Polymer Model, which can be represented by ([23]):

$$\Delta G_{f,sm}^o = \sum n_i \Delta G_{f,i}^o - (\sum n_i Z_i - 12)\Delta G_{f,H_2O}^o - q \tag{4}$$

Where ΔG_f^o refers to the standard Gibbs free energy of formation of the subscripted substance (*sm* = smectite, *i* = a solid hydroxide component containing the *i*th cation occupying an exchange, octahedral or tetrahedral site in smectite, H$_2$O = water), n_i stands for the stoichiometric amount of the component in a half unit cell containing O$_{10}$(OH)$_2$, Z_i represents charge and q refers to a correction factor. The correction factor is needed to account for additional contributions to the Gibbs energy arising from the effects of changes in the coordination environment of exchangeable cations as they are

conceptually transferred from an hydroxide component to an exchange site in the clay.

Equation (4) was evaluated for MX-80 smectite ([21]) using calorimetric and solubility-based $\Delta G^o_{f,i}$ values compiled by [23] and an empirical expression from [26] for the correction factor, which is parameterised in terms of the charges and crystallographic ionic radii of exchangeable cations. The corresponding equilibrium constant for dissolution of MX-80 smectite was then calculated using this estimated $\Delta G^o_{f,sm}$ value and standard partial molal Gibbs free energies of formation for relevant aqueous species taken from the SUPCRT-compatible ([25]) thermodynamic database thermo.com.V8.R6+.dat, which is used in the present study to support calculations using Geochemists Workbench ([27]).

Comparison of the calculations using the Polymer model with those using Vieillard's model are presented in

Table 4 ($\Delta G^o_{f,sm}$) and Table 5 (log K). The difference in Gibbs energies obtained using the two estimation techniques, 16 kJ mol^{-1}, is substantial and results in a difference in the equilibrium constant for the corresponding dissolution reaction of more than two orders of magnitude.

4.3.2 Other minerals, secondary minerals and aqueous species

Thermodynamic data for other minerals in bentonite (calcite, quartz, halite, and gypsum), and aqueous species were taken from the EQ3/6 database 'thermo.com.V8.R6+, and are presented in Table 6. Some model simulations incorporated the precipitation of potential secondary minerals. Thermodynamic data for these minerals are also included in Table 6 and were derived from thermo.com.V8.R6+, except for analcime and phillipsite, with the former from [28], and the latter from [29].

4.4 Kinetics

4.4.1 Smectite

Recent work on montmorillonite dissolution kinetics at elevated pH ([30]; [31]) has been applied in the model simulations. Sato et al. measured the following rate at 30 °C which was used as a reference rate in the time- and space-dependent simulations:

$$rate = 10^{-13.58} \left(a_{H^+} \right)^{-0.15} \tag{5}$$

Table 6. *Summary of thermodynamic data for reactions involving other minerals in bentonite and potential secondary minerals. Data are from the EQ3/6 database thermo.comV8.R6+, except for analcime and phillipsite, with the former from [28], and the latter from [29].*

Mineral	Hydrolysis reaction	log K
Other minerals in bentonite		
Calcite	$CaCO_3 + H^+ = Ca^{2+} + HCO_3^-$	1.8487
Gypsum	$CaSO_4{:}2H_2O = Ca^{2+} + SO_4^{2-} + 2\ H_2O$	-4.4823
Halite	$NaCl = Na^+ + Cl^-$	1.5855
Quartz	$SiO_2 = SiO_{2(aq)}$	-3.9993
Secondary minerals		
Albite	$NaAlSi_3O_8 + 4H^+ = Na^+ + Al^{3+} + 3SiO_{2(aq)} + 2H_2O$	2.7645
Analcime	$NaAlSi_2O_6{:}H_2O + 4H^+ = Na^+ + Al^{3+} + 2SiO_{2(aq)} + 3H_2O$	6.7833
Brucite	$Mg(OH)_2 + 2H^+ = Mg^{2+} + 2H_2O$	16.2980
Chalcedony	$SiO_2 = SiO_{2(aq)}$	-3.7281
Goethite	$FeOOH + 3H^+ = Fe^{3+} + 2H_2O$	0.5345
Kaolinite	$Al_2Si_2O_5(OH)_4 + 6H^+ = 2Al^{3+} + 2SiO_{2(aq)} + 5H_2O$	6.8101
Katoite	$Ca_3Al_2(OH)_{12} + 12H^+ = 3Ca^{2+} + 2Al^{3+} + 12H_2O$	78.9440
Mesolite	$Na_{.676}Ca_{.65}Al_{1.99}Si_{3.01}O_{10}{:}2.647H_2O + 7.96H^+ = .676Na^+ +$ $.65Ca^{2+} + 1.99Al^{3+} + 3.01SiO_{2(aq)} + 6.627H_2O$	13.6191
Phillipsite	$K_{2.8}Na_{3.2}Ca_{0.8}Al_{7.6}Si_{24.4}O_{64}{:}24H_2O + 29.6H^+ =$ $2.8K^+ + 3.2Na^+ + 0.8Ca^{2+} + 7.6Al^{3+} + 24.4SiO_{2(aq)} + 39.2H_2O$	-7.0550
Pyrite	$FeS_2 + H_2O = Fe^{2+} + .25H^+ + 1.75HS^- + .25SO_4^{2-}$	-24.6534
Siderite	$FeCO_3 + H^+ = Fe^{2+} + HCO_3^-$	-0.1920
Tobermorite	$Ca_5Si_6O_{16}(OH)_2{:}4.5H_2O + 10H^+ = 5Ca^{2+} + 6SiO_{2(aq)} + 10.5H_2O$	65.6120

A smectite surface area of 30 m^2 g^{-1} (e.g. [32]) was used in conjunction with this rate.

Rozalén et al. ([31]) describe complete terms for the pH dependency of dissolution rate (at 25 °C):

$$rate = 10^{-12.30} a_{H^+}^{0.40} + 10^{-14.37} + 10^{-13.05} a_{OH^-}^{0.27} \qquad (6)$$

where rate (mol m^{-2} s^{-1}) is given as a function of the activity (*a*) of both protons (H$^+$) and hydroxyls (OH$^-$). Rozalén et al. ([31]) state that their experimental results are consistent with a dissolution mechanism involving inward movement of a dissolution front from crystal edges, the surface area of which has been measured by [33] to be 8.5 m^2 g^{-1} for MX-80 smectite (gas adsorption and AFM measurements), a value which is significantly smaller than that given by BET measurements which also include a contribution for basal planes on the exterior of smectite crystallites. The Rozalén rate was used in the simulations described in the 'reaction kinetics' section and in some of the time- and space-dependent simulations.

4.4.2   Other minerals in bentonite and secondary minerals

In addition to the montmorillonite present in the simplified MX-80 bentonite composition, there are trace amounts of calcite, halite, quartz and gypsum. These minerals are usually modelled using an instantaneous equilibrium assumption, rather than assuming that the reactions are governed by dissolution/precipitation kinetics. For the simulations of the diffusion experiment, the reactions are modelled using a generic kinetic approach based on departure from equilibrium:

$$rate = k.A.\left(1 - \frac{Q}{K}\right) \tag{7}$$

where k is the reaction rate (mol m^{-2} s^{-1}), Q is the ion activity product, and K is the equilibrium constant. Kinetic data are presented in Table 7.

Secondary minerals in some of the simulations of the squeezing experiments were allowed to precipitate at equilibrium (infinite rate), but some simulations of the interaction of high pH fluids with bentonite in a diffusion experiment incorporate kinetic secondary mineral precipitation. A small number of secondary minerals were selected (chalcedony, brucite, phillipsite, analcime, and tobermorite), based on a review of secondary minerals forming during hyperalkaline alteration of clay ([34]). Analcime growth is kinetically inhibited at low temperature, and thus unlikely to form over laboratory experimental timescales ([34]), but was included as a typical mineral likely to form over longer timescales. Kinetic data for these minerals are also presented in Table 7.

4.5   Pore water compositions

Table 8 shows the initial pore water compositions considered in the kinetic and variation in time and space models. Squeezing experiments involved either a dilute fluid ('*L1*'), where the bentonite was initially mixed with deionised water, and most of the $O_{2(g)}$ and $CO_{2(g)}$ was removed by bubbling with $N_{2(g)}$. In the other squeezing experiment, a hyperalkaline fluid ('*L2*'), was produced by bubbling nitrogen through a 1 M NaOH solution. The *L1* and *L2* pore waters referred to in Table 8 were taken after the bentonite samples were squeezed to a dry density of 1.5 Mg m^{-3}. The pH was thereafter continuously monitored for 100 days using an IrOx measurement electrode. In the diffusion experiment, the initial solution was deionised water, which according to Muurinen and Carlsson ([6], [19]) had an initial bentonite-equilibrated pH of 8.4. After 271 days, this solution was replaced by a high pH, high salinity solution for the remainder of the experiment.

Table 7. *Kinetic data for other minerals in bentonite and potential secondary minerals. Surface area values for other minerals in bentonite assume spherical particle geometry and a grain diameter of 100 μm, whereas secondary minerals have a uniform area of 1000 m^2 g^{-1}. In some runs, the area for brucite was reduced to values as low as 0.1 m^2 g^{-1}, to investigate the effects of reduced overall rate. In the absence of measured data for tobermorite and katoite, these have been assigned relatively 'fast' rates of 1e-5 mol m^{-2} s^{-1}.*

Mineral	Log k (mol m^{-2} s^{-1})	A m^2 g^{-1}	p	Source
Other minerals in bentonite				
Halite	-0.21	0.03	-	a
Calcite	-5.2	0.02	-	b
Quartz	-13.40	0.03	-	a
Gypsum	-2.79	0.03	-	a
Secondary Minerals				
Chalcedony	-14.5	1000	-0.52	c
Brucite	-8.24	1000	-	a
Phillipsite	-13.9	1000	-0.36	d
Analcime	-13.9	1000	-0.36	d
Tobermorite	-5.0	1000		e
Katoite	-5.0	1000		e

[a][35]; [b][36]; [c][37]; [d][38]; [e]Estimated.

Table 8. Compositions of the fluids used in the experiments described by [19]. Fluids L1 and L2 are those used in squeezing experiments, whereas DIF6 is that employed in the diffusion experiment. The bicarbonate concentration in the L2 pore water was estimated in the present study based on charge balance constraints. The DIF6 composition is: (a) as described by Muurinen and Carlsson ([6], [19]); and (b) with a calculated bicarbonate content assuming equilibration with calcite. This latter composition implies a low log PCO_2 (-12.15 bars) which could be appropriate for the experimental conditions. The initial concentrations of Al, Si, and Fe are not included in the table and are assumed to be very low (10^{-10} molal). Concentrations are in mg/L.

	L1	L2	DIF6 (a)	DIF6 (b)
pH	9.0	12.1	11.6-11.7	11.7
Na	455	4219	4332	4240
K	129	114	-	-
Ca	12.4	1.9	4005	3924
Mg	6.5	-	-	-
Cl	163	137	10375	10200
SO_4	598	2429		
HCO_3	45.8	6955	-	0.46

5. Model results

Calculations have been carried out to simulate the results of the experiments reported by Muurinen and Carlsson ([6], [19]), namely the 'batch', 'squeezing', and 'diffusion' type. Computer codes employed were 'Geochemists Workbench' ([27]), PHREEQC ([39]), and QPAC ([40]).

5.1 Scoping calculations

In order to determine the extents to which carbonate equilibria, clay hydrolysis, ion exchange and clay edge sites may influence compacted bentonite pore water pH, a series of preliminary batch equilibrium models were constructed using PHREEQC. The models included compacted MX-80 bentonite at a dry density of 1.5 g cm^{-3}. The PHREEQC default water volume is 1 litre (1 kg for pure water). Simplified mineral masses were taken from Table 1 as input and adjusted to give a solid/fluid ratio that represented a bentonite that has an effective porosity of 6 %, corresponding to the 'geochemical' porosity for this clay compaction density described by Muurinen and Carlsson ([6], [19]). The input solution was 1 kg of pure water, into which bentonite minerals were allowed to dissolve to equilibrium with pH being used to charge balance the system and *pe* being unconstrained (i.e. corresponding to redox equilibrium). Input thermodynamic data (log *K* values) were from the PHREEQC database 'llnl', with the exception of MX-80 montmorillonite which was that calculated using the Vieillard Model.

Models 1a-e and 2 included the equilibrium solubility of secondary minerals (calcite, halite, quartz and gypsum) and MX-80 montmorillonite. Cation exchange reactions and protolysis constants were taken from Table 2 and Table 3. The effect of $PCO_{2(g)}$ was investigated by employing a range of different values corresponding to atmospheric and sub-atmospheric levels. In model 2, carbonate equilibria were ignored. Unsurprisingly, calculated pH values varied as a function of $PCO_{2(g)}$ values (Table 9). In the absence of carbonate reactions, the mineral assemblage and ion exchange/protolysis of the montmorillonite resulted in a pH that was 1 unit lower (6.96) than that where calcite was included at log $PCO_{2(g)}$ = -3.5 (7.91).

In models 3a-e, equilibrium pH was calculated in the absence of montmorillonite for a range of $PCO_{2(g)}$ values. The exclusion of montmorillonite resulted in pH values generally being lower than where it was included, with differences ranging from -0.2 pH units at higher $PCO_{2(g)}$ values to +0.05 units at the lowest log $PCO_{2(g)}$ value of -7.5 (Table 9).

In models 4a-e, montmorillonite was included along with secondary minerals, however, it was only allowed to influence solution composition through cation exchange with edge site protolysis (i.e. it was not allowed to dissolve). Calculated pH values are very similar to those of models 1a-e, where montmorillonite was at equilibrium solubility (Table 9).

Table 9. *PHREEQC models of compacted bentonite pore water pH (T = 25 °C, P = 1 bar).*

Model	Input					Output	
	Equilibrium Phases[a]	Surfaces[b]	log p CO$_2$	mass exchanger (g)	mass clay (diss)[c] (g)	pH	I (M)
1a	MX80, cal, hal, qz, gyp	IL + AM	-3.5	coupled to MX80	22650	7.91	0.312
1b	MX80, cal, hal, qz, gyp	IL + AM	-4.5	coupled to MX80	22650	8.36	0.304
1c	MX80, cal, hal, qz, gyp	IL + AM	-5.5	coupled to MX80	22650	8.8	0.309
1d	MX80, cal, hal, qz, gyp	IL + AM	-6.5	coupled to MX80	22650	9.22	0.333
1e	MX80, cal, hal, qz, gyp	IL + AM	-7.5	coupled to MX80	22650	9.64	0.384
2	MX80, hal, qz, gyp,	IL + AM	-	coupled to MX80	22650	6.96	0.350
3a	cal, hal, qz, gyp	-	-3.5	-	-	7.69	0.090
3b	cal, hal, qz, gyp	-	-4.5	-	-	8.19	0.090
3c	cal, hal, qz, gyp	-	-5.5	-	-	8.69	0.090
3d	cal, hal, qz, gyp	-	-6.5	-	-	9.19	0.090
3e	cal, hal, qz, gyp	-	-7.5	-	-	9.69	0.090
4a	cal, hal, qz, gyp	IL + AM	-3.5	22650	-	7.92	0.317
4b	cal, hal, qz, gyp	IL + AM	-4.5	22650	-	8.37	0.308
4c	cal, hal, qz, gyp	IL + AM	-5.5	22650	-	8.81	0.312
4d	cal, hal, qz, gyp	IL + AM	-6.5	22650	-	9.23	0.336
4e	cal, hal, qz, gyp	IL + AM	-7.5	22650	-	9.64	0.384
5a	cal, hal, qz, gyp	IL	-3.5	22650	-	7.99	0.356
5b	cal, hal, qz, gyp	IL	-4.5	22650	-	8.49	0.356

[a]MX-80 = smectite component of MX-80 bentonite; cal = calcite; hal = halite; qz = quartz; gyp = gypsum

[b] IL = smectite interlayer sites; AM = amphoteric crystal edge sites

[c]Mass of smectite allowed to undergo hydrolysis (per kg of pure water – see text for details).

In models 5a and 5b, edge site protolysis was not included, which resulted in calculated pH values being 0.9 and 0.14 units higher than in models 4a and 4b (at log $PCO_{2(g)}$ values of -3.5 and 4.5 respectively). The models which included edge site protolysis reactions include the following input variables: moles of site for the mass of montmorillonite present, moles of site/moles of montmorillonite and surface area of the sites. In the models presented here, a surface area of 8.5 m^2 g^{-1} was used (corresponding to edge sites only). If a larger BET surface area is used (31.3 m^2 g^{-1}), the pH for model 4a is lower (7.86 as opposed to 7.95 units), highlighting the importance of measured/modelled surface area data.

5.2   Consideration of reaction kinetics

It is conceivable that even very slow smectite dissolution rates could affect the geochemical evolution of the buffer given the long periods of time that are relevant to safety assessments of a KBS-3 repository. This possibility is evaluated below using a simplified kinetic model of smectite dissolution (Rozalén model – equation (6) + Polymer model thermodynamic data) in a closed bentonite-water system at dry densities envisaged for the buffer (≈ 1.5 Mg m^{-3}).

This model is evaluated under three limiting conditions: model A - dissolution of MX-80 smectite for 100 days at 25°C, 1 bar (all other mineral dissolution/precipitation reactions are ignored); model B - continuation of model A to the time when r = 0 (equilibrium); and model C - extension of Model B to include (equilibrium) precipitation of selected secondary phases.

Calculated changes in the amount of smectite dissolved in dilute pore water (Experiment *L1*) and in 1 M NaOH (Experiment *L2*) over a period of 100 days (Model A) were minimal (Figure 8) and the compositions of both aqueous solutions remained at conditions far from equilibrium (Figure 9), and the dissolution rate was therefore essentially controlled only by the rate constant and surface area, and, at pH > 10, by a_{OH^-}. Resultant changes in pH (Figure 10) were controlled by the dissolution rate and by hydrolysis of the released cations. Smectite dissolution consumes H^+, whereas cation hydrolysis produces H^+ (e.g., $Al^{3+} + 4H_2O(l) = Al(OH)_4^- + 4H^+$). The net result is a small reduction in pH in both the *L1* (-0.005 pH units) and *L2* (-0.001 pH units) solutions. These changes are much smaller than those observed experimentally (-0.2 and -2.5 pH units for *L1* and *L2*, respectively), which confirms that smectite dissolution is a process of minor importance under laboratory timescales at neutral pH.

We next consider changes in solution chemistry that would occur if smectite were to continue to dissolve beyond 100 days up until the time equilibrium is achieved. The calculated amounts dissolved and corresponding changes in pH are shown in Figure 11 and Figure 12, respectively. As can be seen in the former, 7.2 years are required for equilibrium in *L1*, and 65 years in *L2*. Both durations are much longer than the experiments of [6]. Changes in pH are small (Figure 12), again suggesting that the effects of smectite dissolution are relatively unimportant under these conditions.
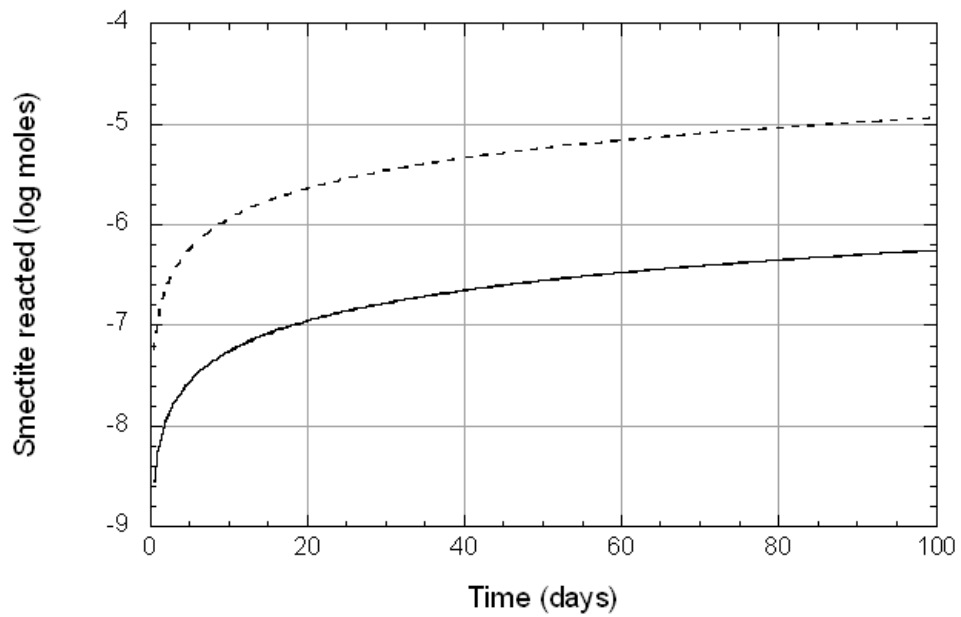
Figure 8. *Calculated amounts of smectite dissolved in L1 pore water (solid line) and L2 pore water (dashed line) over a period of 100 days at 25°C, 1 bar.*
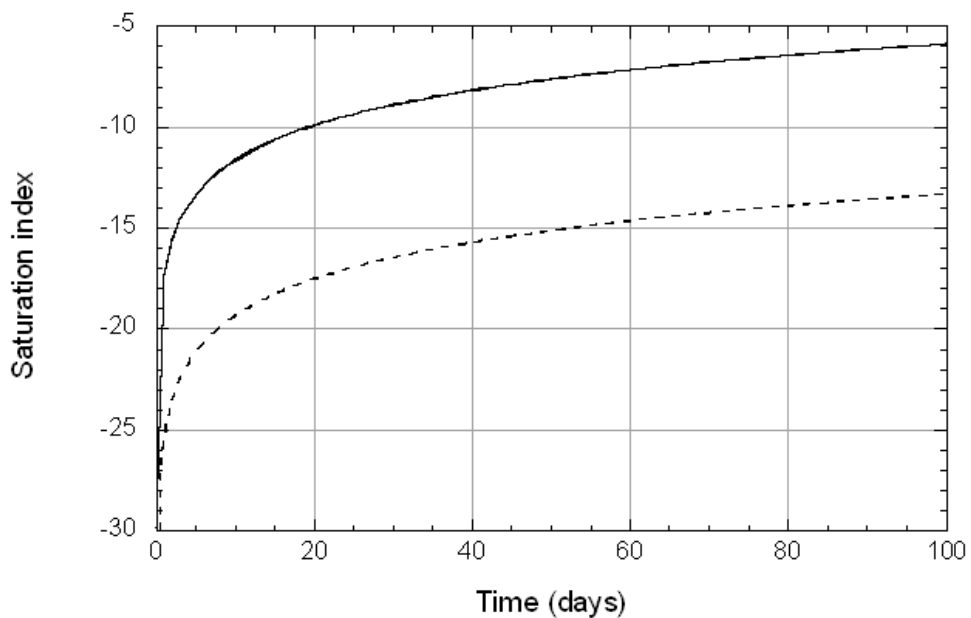

Figure 9. *Calculated variations in the saturation index for smectite dissolution in L1 pore water (solid line) and L2 pore water (dashed line) as a function of time at 25°C, 1 bar.*
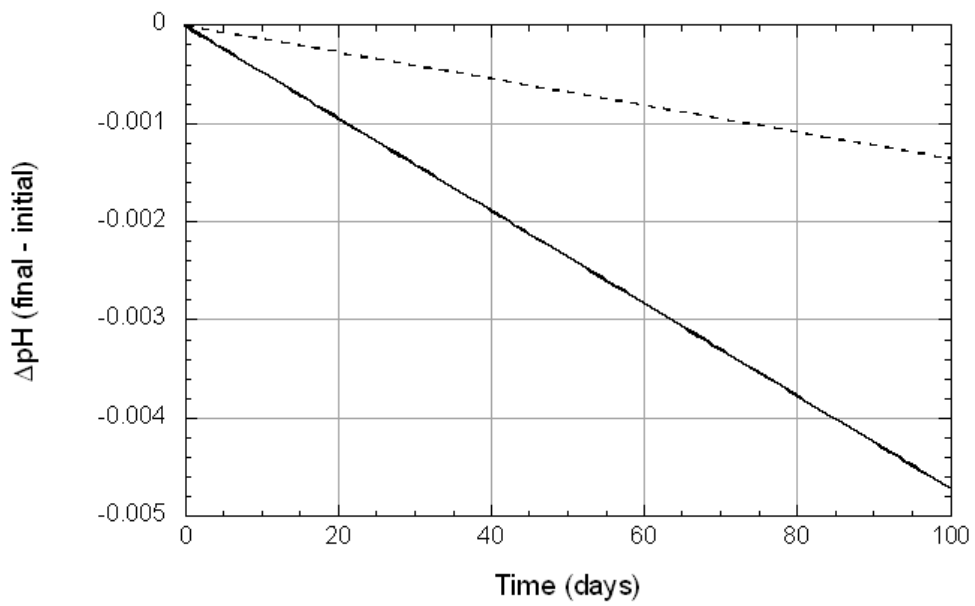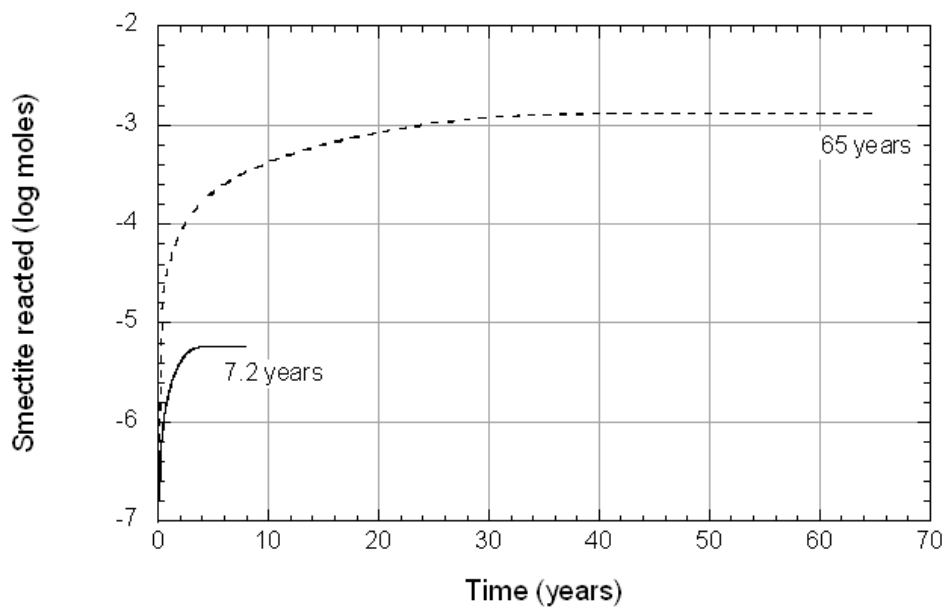
Figure 10. *Calculated differences in pH during smectite dissolution in L1 pore water (solid line; initial pH = 9) and L2 pore water (dashed line; initial pH = 12.1) as a function of time at 25°C, 1 bar.*

Figure 11. *Calculated amounts of smectite dissolved in L1 pore water (solid line) and L2 pore water (dashed line) over time periods required to achieve equilibrium (indicated by symbols) at 25°C, 1 bar.*
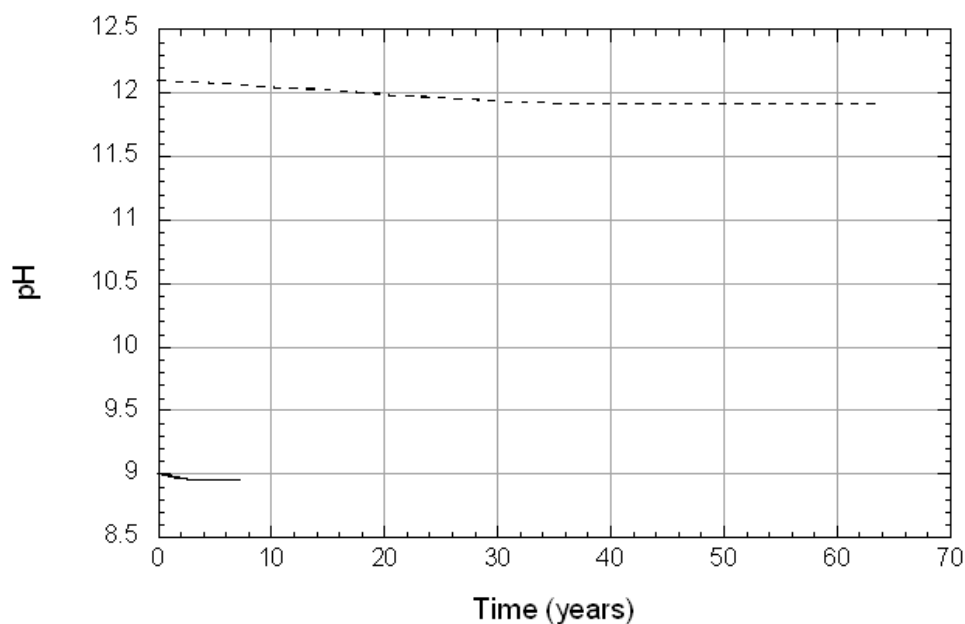
Figure 12. *Calculated variations in pH as L1 pore water (solid line) and L2 pore water (dashed line) approach equilibrium with smectite at 25 °C, 1 bar (Model B).*

Models A and B both assume that secondary minerals do not precipitate as smectite dissolves. Figure 13 indicates, however, that the aqueous concentrations of Al, Fe and Si increase significantly as smectite approaches equilibrium with the *L1* and *L2* pore waters (Model B). Given these changes in solution chemistry, it seems reasonable to expect that insoluble secondary minerals (e.g. oxides, hydroxides, carbonates, aluminosilicates) will precipitate as smectite dissolves. This latter possibility is evaluated in Model C which represents a variant of Model B with the added provision that plausible secondary minerals are allowed to precipitate under local equilibrium control if solution compositions evolve accordingly. The secondary minerals considered in Model C are: kaolinite, calcite, goethite and sepiolite (representing a generic, insoluble Mg-bearing silicate) (*L1* pore water); and analcime, albite, goethite, sepiolite, mesolite, siderite and pyrite (*L2* pore water). Thermodynamic data for these minerals are included in Table 6. Given the general insolubility of aluminosilicate and other common types of secondary minerals, however, these illustrative effects are expected to be qualitatively similar to those that would be predicted using more realistic (kinetic) models of bentonite-pore water interactions. Goethite and pyrite are included in Model C because MX-80 smectite contains small amounts of both ferrous and ferric iron. Redox conditions are further constrained by assuming that the model system initially equilibrates with atmospheric $O_{2(g)}$ with $pO_{2(g)} = 0.21$ bar.
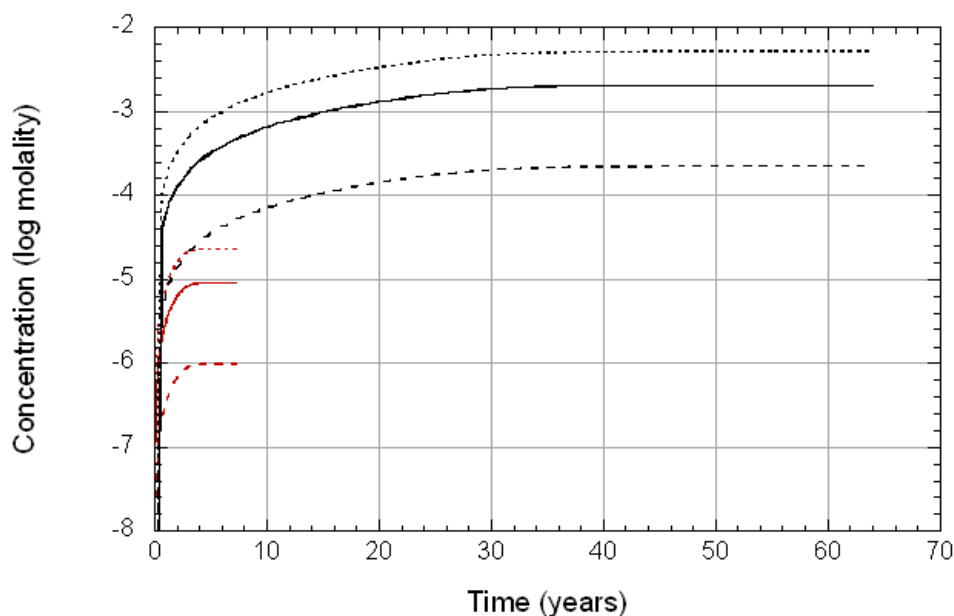
Figure 13. *Calculated changes in the concentrations of Al^{3+} (solid lines), ΣFe (dashed lines) and SiO$_2$(aq) (dotted lines) during dissolution of MX-80 smectite in dilute (L1) pore water (red lines) and 1 M NaOH (black lines). The terminus of each curve represents conditions at equilibrium (see Figure 11). Initial cation concentrations = 10^{-10} molal.*

Figure 14 and Figure 15 depict changes in the amounts of smectite dissolved and secondary minerals precipitated as smectite equilibrates with the *L1* and *L2* pore waters, respectively. A striking feature of both Figures is that equilibration times are much longer than those predicted using Model B (360 years versus 7.2 years for *L1* pore water; 2600 years versus 65 years for *L2* pore water). Corresponding changes in pH (Figure 16) are also much more pronounced than those calculated using Model B. These results indicate that when the kinetic model of smectite dissolution is combined with plausible local-equilibrium constraints on the precipitation of secondary phases, predicted changes in solution chemistry can be significant.

The Model C variant involving *L2* pore water was further evaluated using an alternative value for the log *K* for hydrolysis of MX-80 smectite that was estimated using the approach of Vieillard ([22]). Results are shown in Figure 17 and Figure 18. The use of log *K* estimated using Vieillard's technique (log *K* = 4.4) in place of that estimated using the Polymer model (log K = 2.07) causes the time required for MX-80 smectite to equilibrate to increase from 2600 years to 5000 years. Changes in pH using these two different log *K* values are identical under far-from-equilibrium conditions, but differ significantly as equilibrium is approached (Figure 18*)*. The differences reflect uncertainties in the thermodynamic properties of smectite. The results shown in Figure 18 suggest that this uncertainty can significantly affect models of the kinetic evolution of smectite-water reactions.
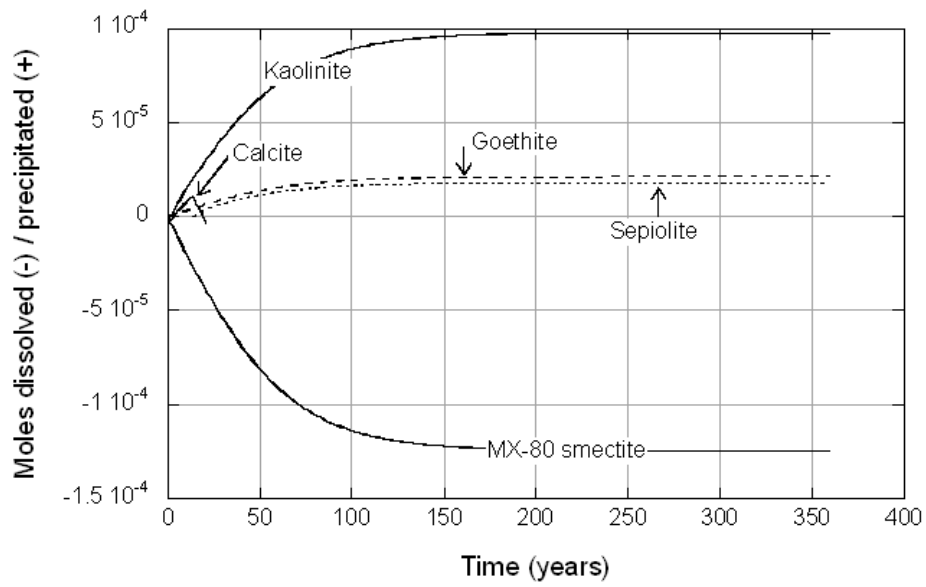
Figure 14. *Variations in mineral abundances as dilute (L1) pore water equilibrates with MX-80 smectite. Equilibration time = 360 years.*
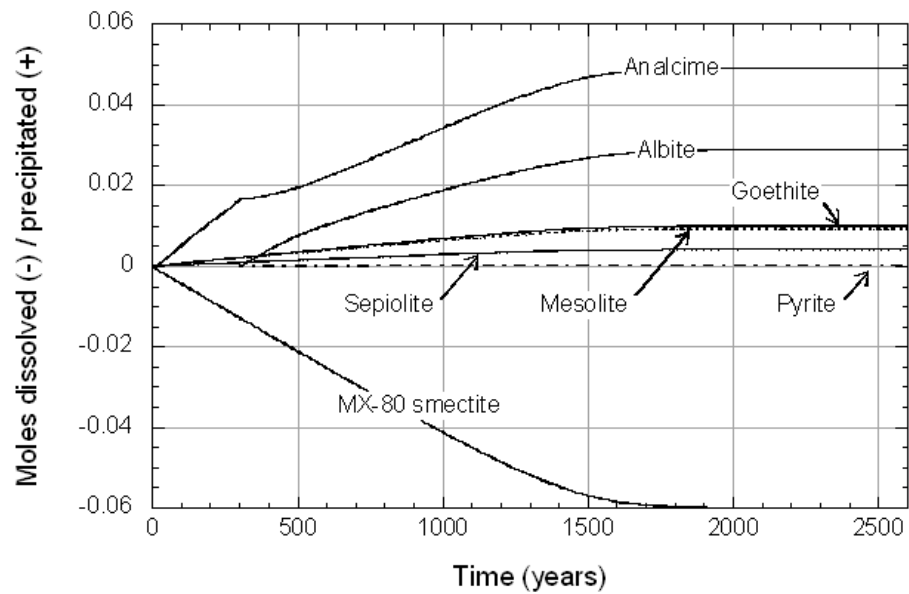

Figure 15. *Variations in mineral abundances as alkaline (L2) pore water equilibrates with MX-80 smectite. Equilibration time = 2600 years.*
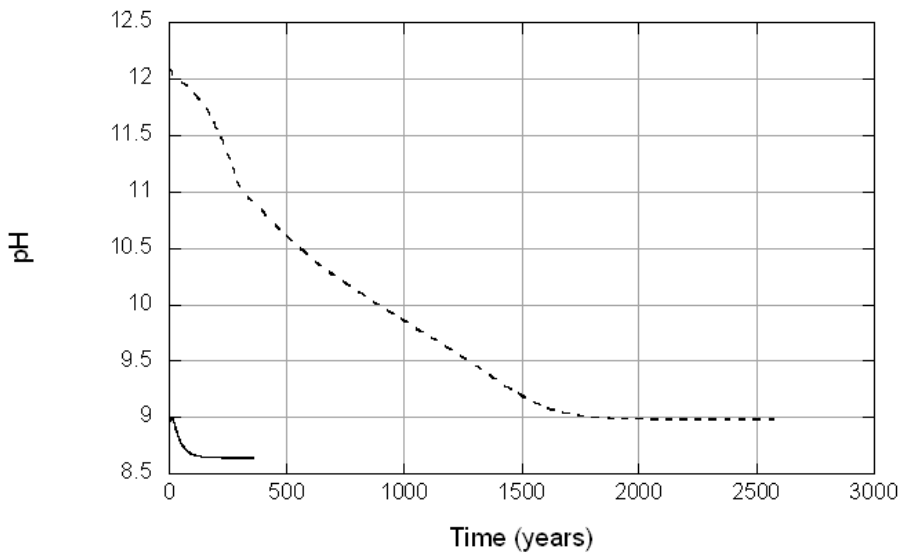
Figure 16. *Calculated changes in pH as L1 pore water (solid line) and L2 pore water (dashed line) approach equilibrium with smectite at 25 °C, 1 bar (Model C).*
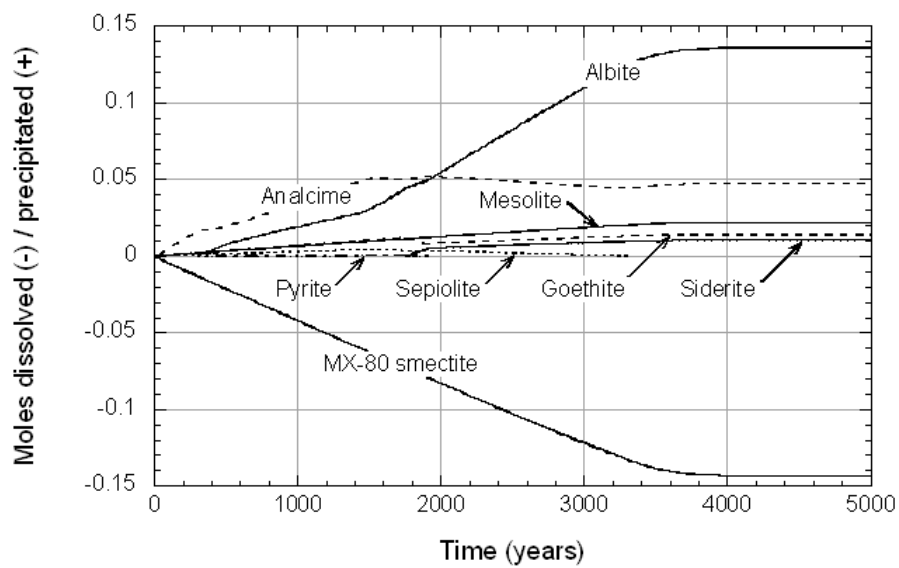

Figure 17. *Variations in mineral abundances as alkaline (L2) pore water equilibrates with MX-80 smectite. The equilibrium constant for smectite dissolution estimated using the model of Vieillard ([22]) was used in this simulation in place of that estimated using the Polymer Model. Equilibration time = 5000 years.*
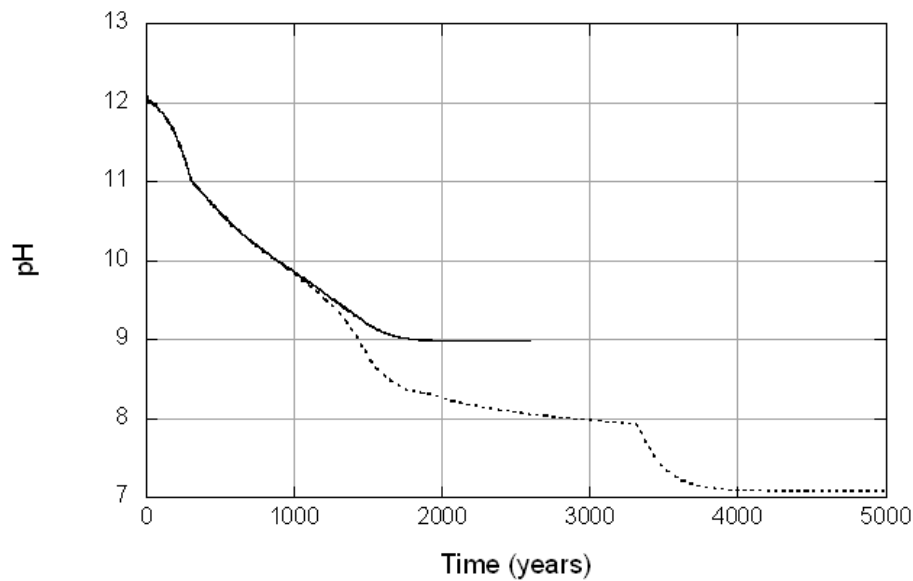
Figure 18. *Comparison of pH evolution calculated in Model C (L2) using alternative log K values for MX-80 smectite dissolution. The solid line refers to calculations based on the Polymer Model (log K = 2.07), and the dashed line refers to calculations based on Vieillard's technique (log K = 4.89).*

5.3   Time- and space-dependent calculations

The diffusion experiment 'DIF6' of Muurinen and Carlsson ([6], [19]) was modelled in time and space using the QPAC computer code ([40]), which has a fully coupled reactive-transport chemical module. A number of cases were set up and run, to investigate the effects of individual processes (such as secondary mineral precipitation, ion exchange etc.) on the system. A summary of the model cases is given in Table 10.

QPAC employs a finite volume approach. The model of the diffusion experiment was discretised using 19 compartments in the bentonite, ranging from 0.5 mm wide at the end exposed to the high-pH fluid, to 10 mm at the most distal end. The fluid reservoir was modelled as a single compartment. In order to represent the changes to the high-pH fluid in the reservoir, and the subsequent replenishment of the reservoir fluid, 7 separate reservoir compartments were used which were each connected to the bentonite in sequence (by turning fluxes on and off). For the majority of cases considered, a very short diffusion length in the reservoir was considered (0.01 mm); however this did not always provide the best fit to the data, and was thus varied in some variant cases (to 1 mm or even 40 mm). This parameter can be thought of as quantifying how well-mixed the reservoir is; the shorter the length, the better mixed it is. Results from a selection of the model cases are discussed in the following sections.

Table 10. *Summary of the model cases for the diffusion experiment DIF6.*

Case	Secondary minerals	Ion Ex-change	Surface Com-plexation	Porosity Model	Analcime?	Brucite Surface Area	Reservoir mixing length	Smectite kinetics	CO$_{2(aq)}$?	Diffusion Coefficient
D	×	×	×	Total	N/A	N/A	0.01 mm	Sato	×	7.42e-11 m^2 s^{-1}
E1	✓	×	×	Total	✓	1e3 m^2 g^{-1}	0.01 mm	Sato	×	7.42e-11 m^2 s^{-1}
E2	✓	×	×	Total	×	1e3 m^2 g^{-1}	0.01 mm	Sato	×	7.42e-11 m^2 s^{-1}
F	✓	×	×	Geochemical	✓	1e3 m^2 g^{-1}	0.01 mm	Sato	×	7.42e-11 m^2 s^{-1}
G1	✓	✓	×	Total	✓	1e3 m^2 g^{-1}	0.01 mm	Sato	×	7.42e-11 m^2 s^{-1}
G2	✓	✓	×	Total	×	1e3 m^2 g^{-1}	0.01 mm	Sato	×	7.42e-11 m^2 s^{-1}
H1	✓	✓	×	Total	✓	0.1 m^2 g^{-1}	0.01 mm	Sato	×	7.42e-11 m^2 s^{-1}
H2	✓	✓	×	Total	×	0.1 m^2 g^{-1}	0.01 mm	Sato	×	7.42e-11 m^2 s^{-1}
J1	✓	✓	×	Total	✓	0.1 m^2 g^{-1}	1 mm	Sato	×	7.42e-11 m^2 s^{-1}
J2	✓	✓	×	Total	×	0.1 m^2 g^{-1}	1 mm	Sato	×	7.42e-11 m^2 s^{-1}
K1	✓	✓	×	Total	✓	0.1 m^2 g^{-1}	40 mm	Sato	×	7.42e-11 m^2 s^{-1}
K2	✓	✓	×	Total	×	0.1 m^2 g^{-1}	40 mm	Sato	×	7.42e-11 m^2 s^{-1}
L1	✓	✓	×	Geochemical	✓	0.1 m^2 g^{-1}	0.01 mm	Sato	×	7.42e-11 m^2 s^{-1}
L2	✓	✓	×	Geochemical	×	0.1 m^2 g^{-1}	0.01 mm	Sato	×	7.42e-11 m^2 s^{-1}
M1	✓	✓	×	Total	✓	0.1 m^2 g^{-1}	0.01 mm	Rozalen	×	7.42e-11 m^2 s^{-1}
M2	✓	✓	×	Total	×	0.1 m^2 g^{-1}	0.01 mm	Rozalen	×	7.42e-11 m^2 s^{-1}
N1[a]	✓	✓	×	Total	×	0.1 m^2 g^{-1}	0.01 mm	Sato	✓	7.42e-11 m^2 s^{-1}
N2[b]	✓	✓	×	Total	×	0.1 m^2 g^{-1}	0.01 mm	Sato	✓	7.42e-11 m^2 s^{-1}
Q	✓	✓	×	Total	×	0.1 m^2 g^{-1}	0.01 mm	Sato	✓	7.42e-12 m^2 s^{-1}
R[c]	✓	×	✓	Total	✓	1e3 m^2 g^{-1}	1 mm	Sato	×	7.42e-11 m^2 s^{-1}

[a] Initial CO$_2$(aq) concentration was $10^{-4.5}$ mol l^{-1}.

[b] Initial CO$_2$(aq) concentration was $10^{-3.5}$ mol l^{-1}.

[c] The pH of the deionised water was artificially fixed at 8.4. Montmorillonite surface area increased by a factor of 10 (was 30 m^2 g^{-1}); that of analcime reduced to 18 m^2 g^{-1} (from 1000 m^2 g^{-1}).

5.3.1 Case D – smectite hydrolysis only

In this case (the simplest of all the cases considered), the only process included was the hydrolysis of the primary minerals, using the kinetic data of Sato et al. ([30]) which formed the reference dataset for clay dissolution kinetics for the time- and space-dependent modelling. Figure 19 shows the evolution of pH at each of the measurement points in the sample and in the reservoir (symbols and dotted lines show the measured values, solid lines show the model output). As might be expected (and in support of calculations described for Model A), there is no buffering of the pH and the whole system rapidly reaches a state of equilibrium such that the pH is the same throughout the sample and in the reservoir.

5.3.2 Cases E1 and E2 – inclusion of secondary mineral growth

The additional process of kinetic secondary mineral precipitation was included in this case. If analcime is allowed to precipitate, the effect on the pH in the bentonite sample is marked, with a sharp decrease in pH (Figure 20). The pH at 5 mm depth remains between 9.5 and 10, but deeper into the sample, pH decreases (fluctuating between about 7.5 and 9 as it responds to the replenishing of the reservoir). The modelled pH in the reservoir matches the experimental data well; in the bentonite sample the model only captures some of the most basic behaviour, though it is clear that the precipitation of secondary minerals is an important process in the buffering of the pH. A volume fraction plot for this case is shown in Figure 21 after 2 years of simulation. The high pH reservoir is located at the right-hand end of the plot. Large amounts of montmorillonite have dissolved in the first few millimetres, replaced by analcime and tobermorite.

Over lab timescales at 25 °C, it is thought unlikely that analcime will form. Therefore a second simulation was performed with this mineral removed; the pH evolution is shown in Figure 22. Although the pH is buffered a little compared to the case with no secondary mineral precipitation (c.f. Figure 19), the evolution at depth in the bentonite mirrors that at 5 mm. The most abundant mineral is tobermorite (with small amounts of brucite).

5.3.3 Case F – geochemical porosity model

A discussion of porosity models was given in Section 2. The previous runs used the total porosity; for this case the effects of using the 'geochemical' porosity are studied. Agreement with the experimental results was not good; the pH at all points in the bentonite decreased to a very low value (~7.5) after an initial spike in response to the introduction of high-pH fluid from the reservoir (Figure 23). This is due to the precipitation of the analcime and tobermorite which quickly blocks the limited porosity, inhibiting the transport of ions through the sample.
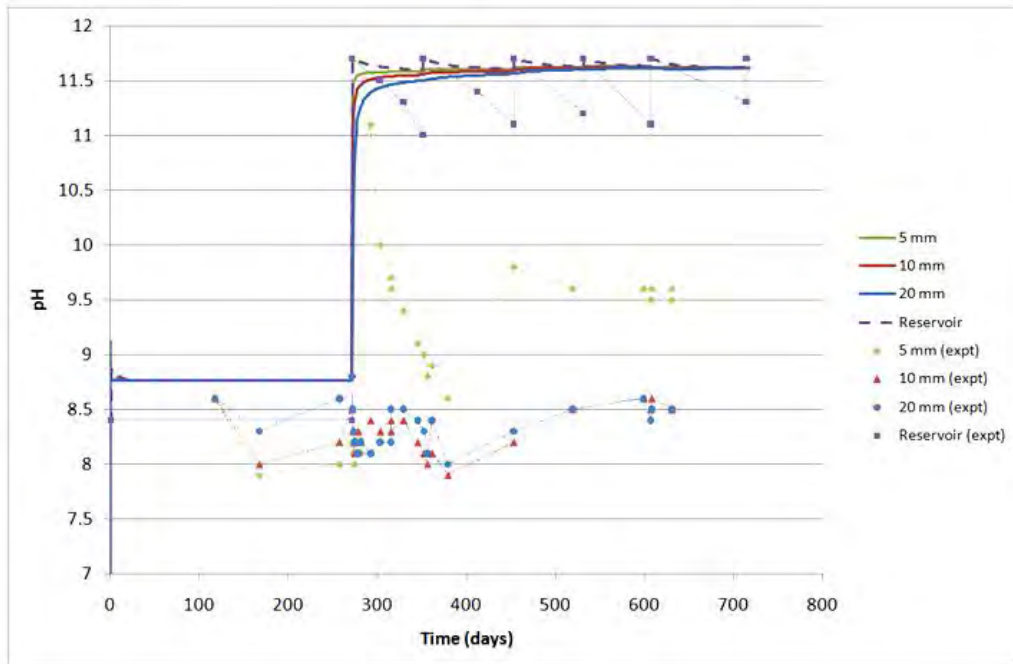
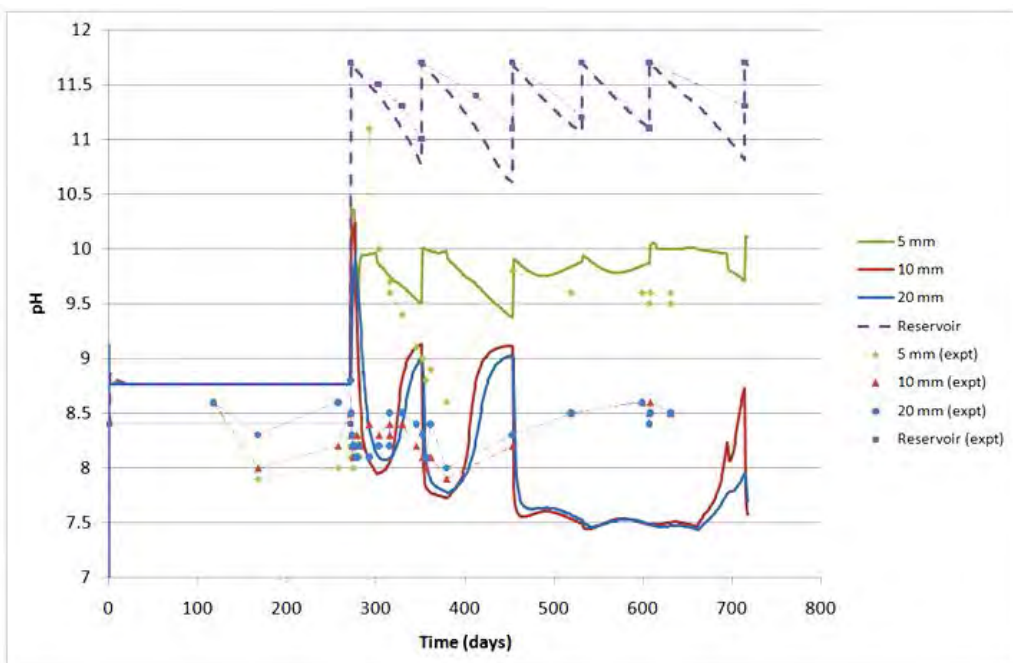*Figure 19.* The evolution of pH for Case D (only mineral hydrolysis included).

Figure 20. The evolution of pH for Case E1 (primary mineral hydrolysis and secondary mineral precipitation).
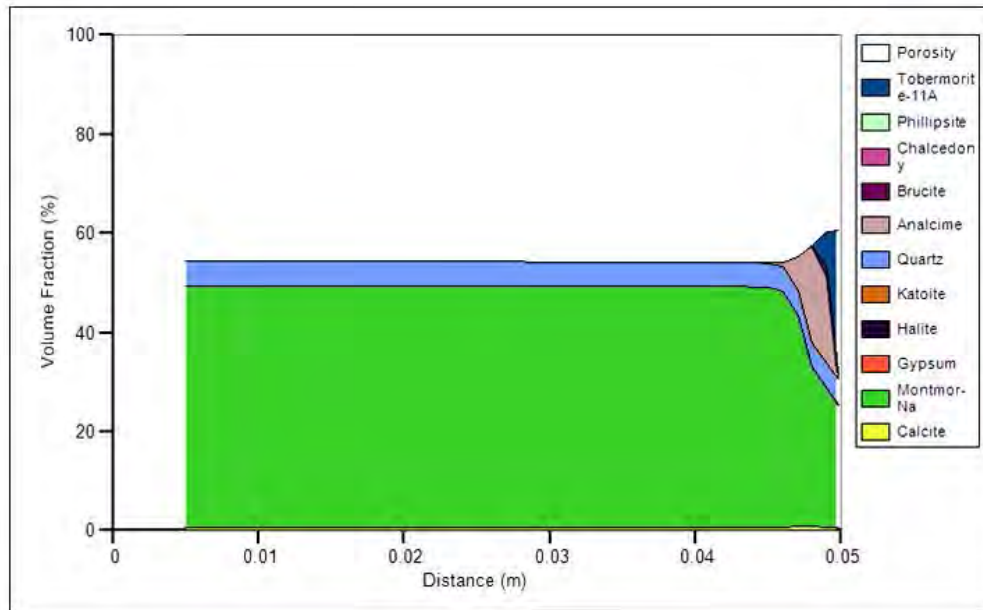
Figure 21. *Volume fraction plot for Case E1 at 2 years. The montmorillonite has dissolved near the incoming high-pH water (right-hand end); analcime and tobermorite have precipitated in its place.*
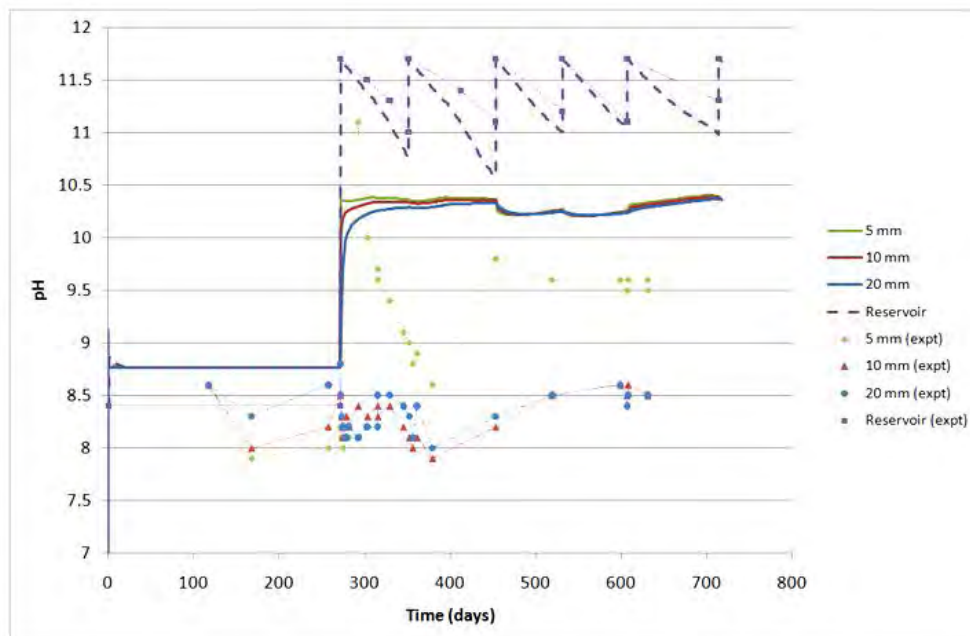

Figure 22. *The evolution of pH for Case E2 (primary mineral hydrolysis and secondary mineral precipitation, no analcime).*
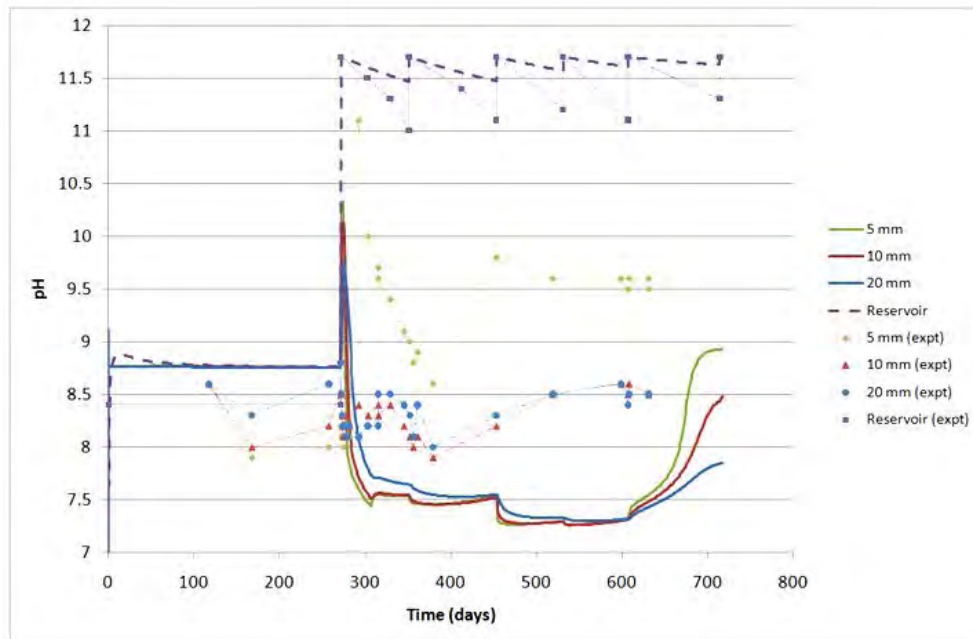
Figure 23. The evolution of pH for Case F (primary mineral hydrolysis, secondary mineral precipitation, and geochemical porosity).

5.3.4 Cases G1 and G2 – inclusion of ion exchange

These cases included ion exchange on the clay, as well as kinetic clay hydrolysis and kinetic secondary precipitation (reverting to use of the total porosity). If analcime is included as a secondary mineral, there is a poor fit to the experimental data (Figure 24). In this case, brucite precipitates in larger quantities, along with analcime and tobermorite.

If analcime is omitted from the calculations, the results are closer to measured values (Figure 25), but there is no initial spike in pH at 5 mm, and the pH values at 10 and 20 mm are greater than those measured. It is also noted that the pH of the reservoir is too low, especially near the start of the simulation.
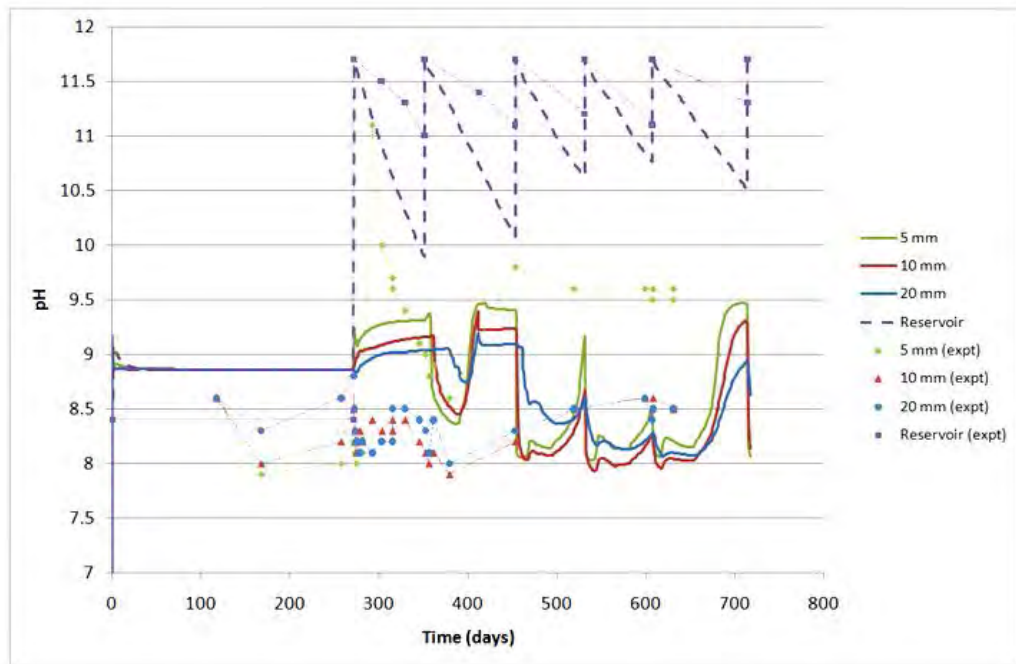
Figure 24. The evolution of pH for Case G1 (primary mineral hydrolysis, secondary mineral precipitation and ion exchange).
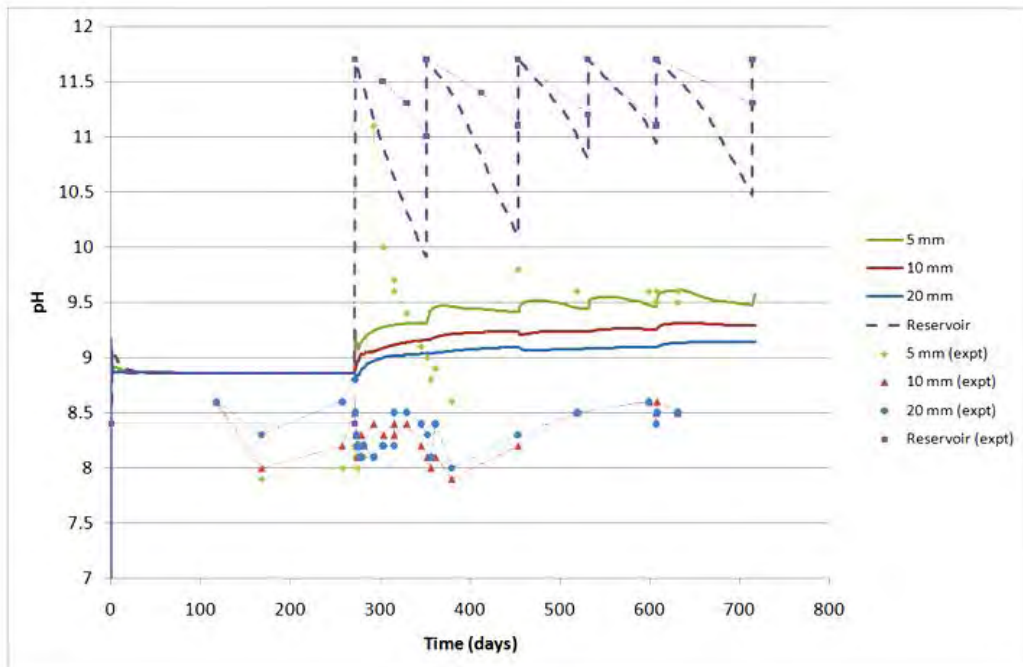

Figure 25. The evolution of pH for Case G2 (primary mineral hydrolysis, secondary precipitation and ion exchange, no analcime).
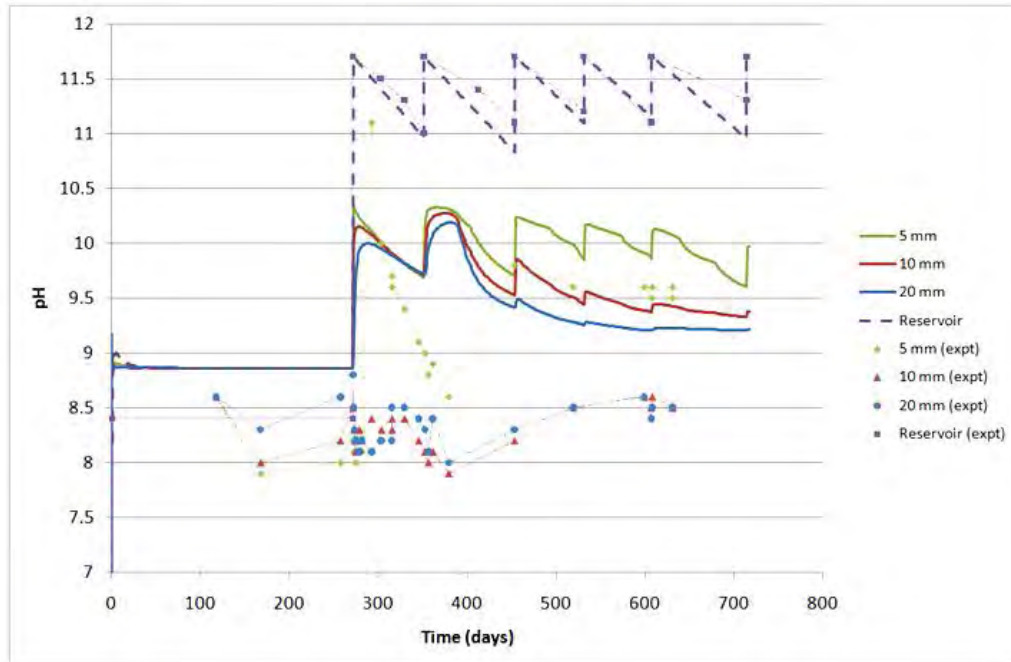
Figure 26. *The evolution of pH for Case 6a (primary dissolution, secondary mineral precipitation, ion exchange, slower brucite precipitation and a less well-mixed reservoir; no analcime).*

5.3.5   Case J – increased reservoir mixing length

The 'saw-tooth' variation of pH in the reservoir reflects the periodic replenishment of the high pH fluid and then decrease of pH due to reaction-diffusion. By increasing the diffusion length in the reservoir to 1 mm (from 0.01 mm), it is possible to obtain a better fit to the pH evolution. In addition, it was found that the precipitation of brucite was very important in buffering the pH. Too much brucite and the pH was held at a low value throughout the bentonite (e.g. Figure 25); too little and there was no buffering capacity (e.g. Figure 19). Figure 26 shows the results from a case where the specific surface area of brucite has been reduced to 0.1 m^2 g^{-1} (from 1000 m^2 g^{-1}), slowing its reaction rate.

Although the simulation results remain an indifferent fit to the experimental data, some of the basic features are observed, e.g. an initial peak in pH and a buffering capability, with less response deeper into the bentonite (at least after ~500 days).

5.3.6 Case M – alternative kinetic model for smectite

For this case, an alternative dataset for clay dissolution ([31]) was employed to describe the dissolution of montmorillonite (equation (6)). Ion exchange was also included, and the rate of brucite precipitation decreased as for case J. There was little difference between the pH evolution for this case and that for case J2, although the peaks in pH were larger and smoother in case M2 (Figure 27). However, a volume fraction plot (Figure 28) indicates that, after 2 years, there is negligible montmorillonite dissolution. Brucite is the dominant secondary mineral.

5.3.7 Case N – inclusion of $CO_{2(aq)}$

A recurring feature of all the cases is that the initial pH in the bentonite is too great (about 9 compared to the value between 8 and 8.5 measured in the experiments). Although the experiment was conducted in a nitrogen glove box, and thus theoretically with the exclusion of CO_2, the reported pH does not seem to be consistent with a system with CO_2 excluded. To test this, $CO_{2(aq)}$ was introduced as an aqueous species with a concentration of $10^{-4.5}$ mol l^{-1} in the initial deionised water. In the high-pH water, it was taken to be at trace concentration. Model results showed that pH evolution is similar to case J2 (Figure 29), but as expected, the initial pH matches the experimental results more closely. Changes in calcite concentrations were minor in all runs and thus had negligible impact upon pH in accord with its dissolution reaction at elevated pH:

$$CaCO_3 = Ca^{2+} + CO_3^{2-} \qquad (7)$$

5.3.8 Case Q – reduction of diffusion coefficient

For this case, the pore water diffusion coefficient was reduced by an order of magnitude to 7.42e-12 $m^2 s^{-1}$. As shown in Figure 30, this has the effect of enhancing the first peak in the pH in the bentonite and smoothing out those at later times, fitting the experimental results at 5 mm far better than the previous cases. However, the pH deeper into the bentonite also behaves in a similar manner, unlike the experimental results. Also, there is a poor fit to the measured pH in the reservoir.
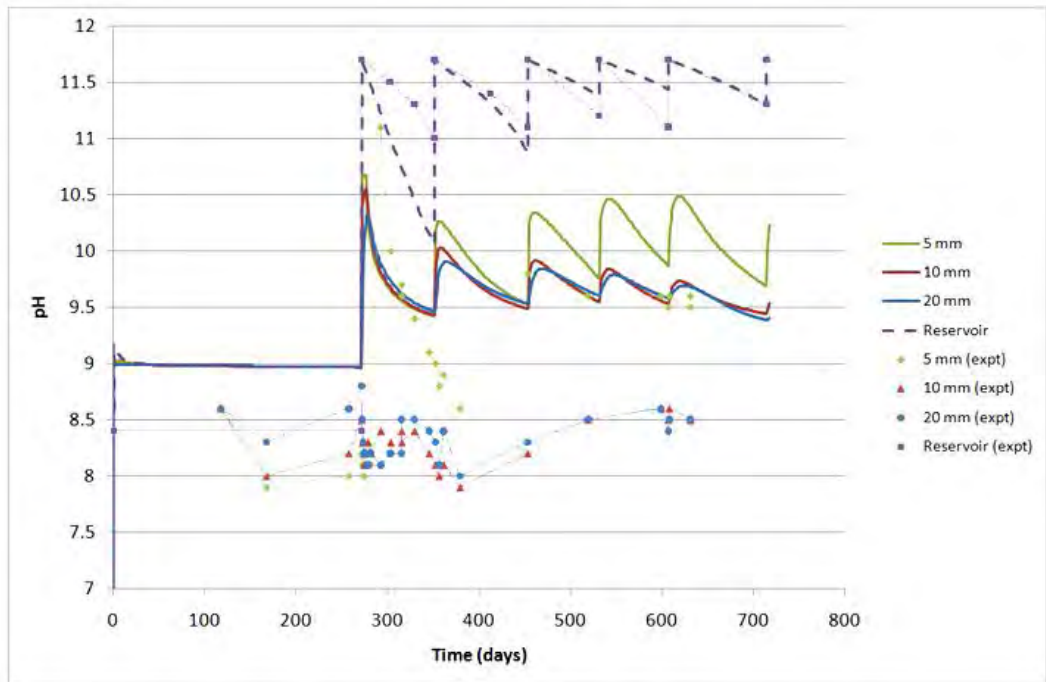
Figure 27. *The evolution of pH for Case M2 (primary mineral hydrolysis, secondary mineral precipitation, ion exchange, slower brucite precipitation and Rozalén model for montmorillonite dissolution; no analcime).*
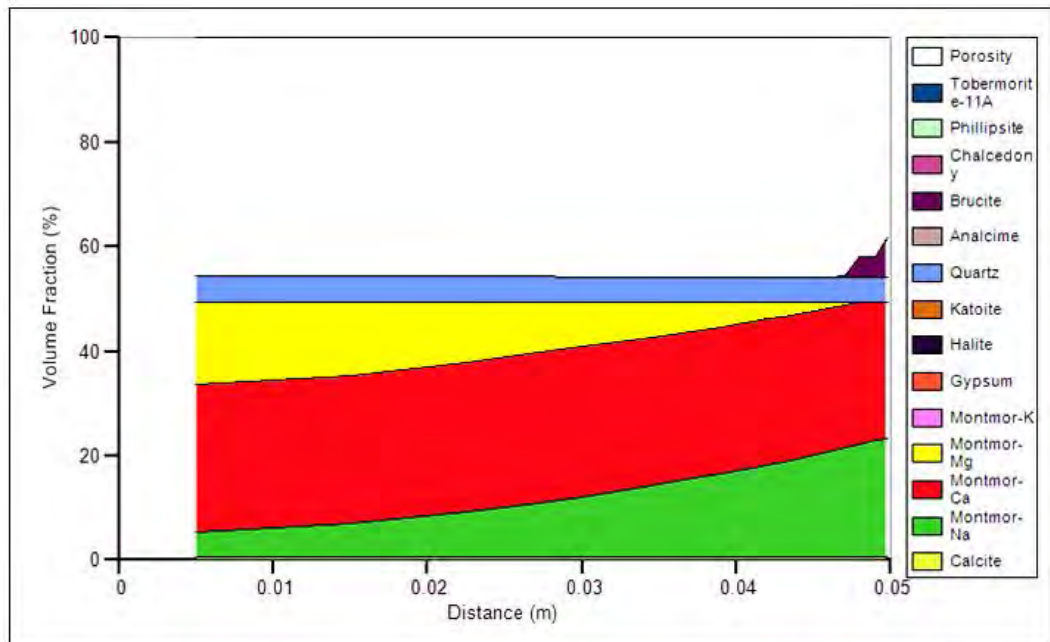

Figure 28. *Volume fraction plot for Case M2 at 2 years. There is negligible montmorillonite dissolution; brucite is the only mineral to form in significant quantities near the inflowing high-pH water (right-hand end). Note the progression of ion exchange across the bentonite.*
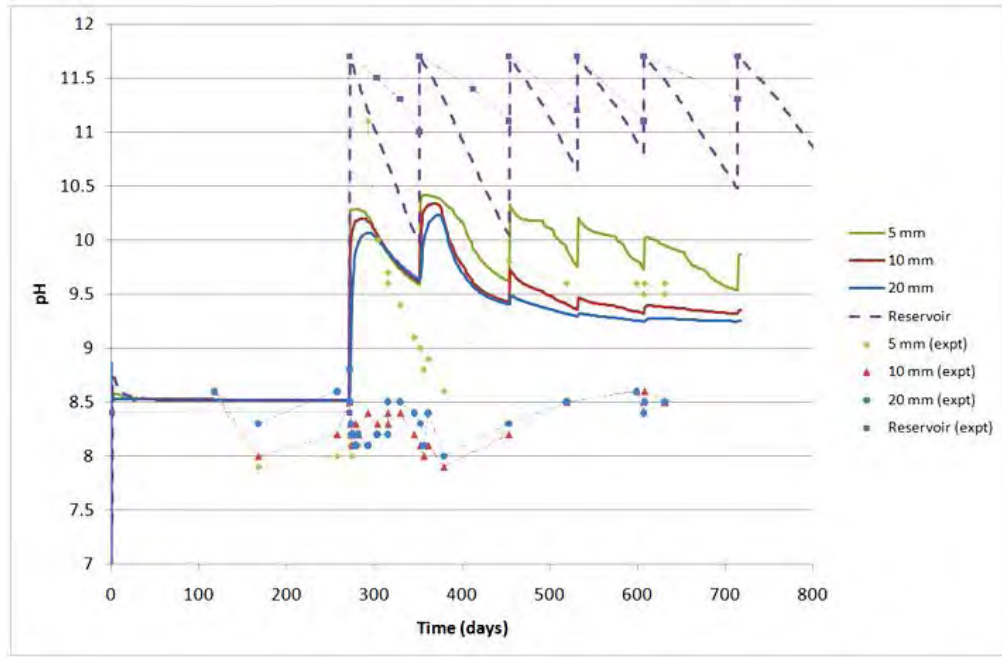
Figure 29. *The evolution of pH for Case 10 (primary dissolution, secondary mineral precipitation, ion exchange, slower brucite precipitation and $CO_{2(aq)}$ included with an initial concentration of $10^{-4.5}$ mol l^{-1}).*
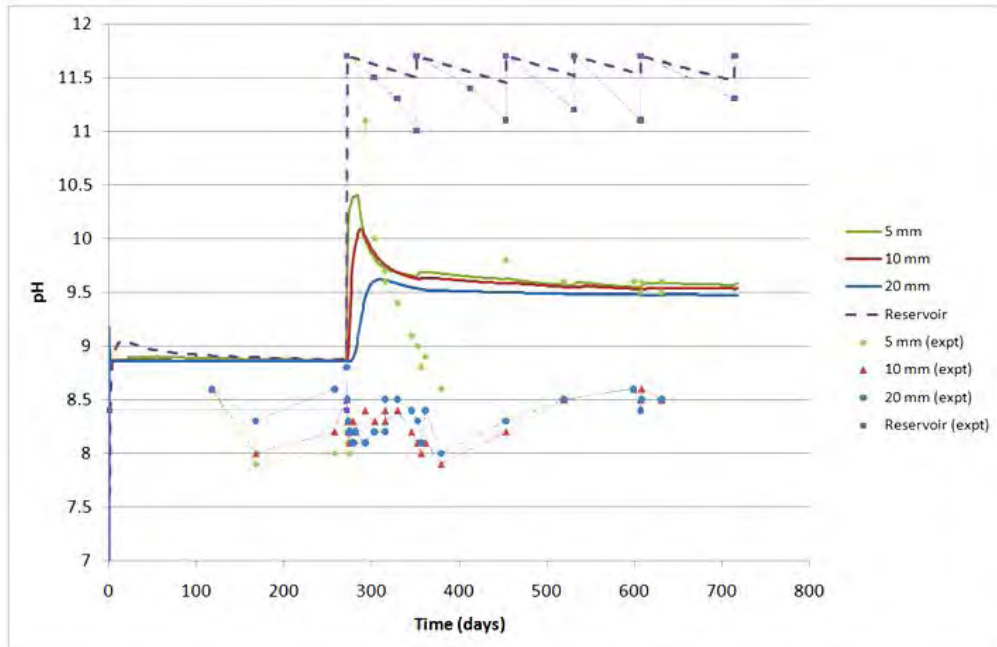

Figure 30. *The evolution of pH for Case 12 (primary dissolution, secondary precipitation, ion exchange, slower brucite precipitation and slower diffusion, no analcime).*
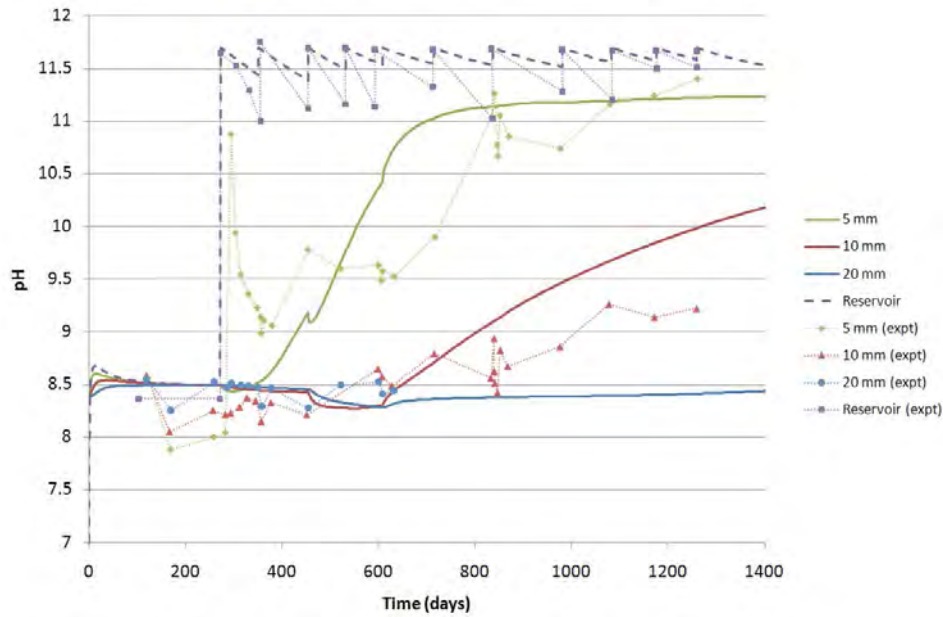
Figure 31. *The evolution of pH for Case 13 (primary dissolution, secondary mineral precipitation, surface complexation, ion exchange excluded, slowed analcime precipitation, and less well-mixed reservoir).*

5.3.9 Case R – exclusion of ion exchange

For this case, ion exchange was excluded, but surface complexation was introduced. In order to better fit the experimental data, the pH of the deionised water was fixed at 8.4 and a diffusion length of 1 mm was used for the reservoir. In addition, the dissolution rate of montmorillonite was increased by making the specific surface area an order of magnitude larger (300 m^2 g^{-1}) than for the previous cases, whereas analcime was excluded from the potential secondary minerals.

Of all the cases considered, perhaps this best captures the basic features of the experiment (Figure 31). There is very little response in the pH at 20 mm depth in the bentonite, whilst at 5 mm, there is reasonable match to the increase in pH after 800 days. The initial spike in pH at 300 days at 5 mm depth in the experiment is not reproduced in the model which suggests that the experimental data may be an artefact. The ramping up of pH after approximately 700 days at 10 mm depth in the experiment is matched reasonably well by the model. Experimental data at 20 mm depth cease after 600 days due to electrode failure and the model suggests that pH at this depth does not respond to increased pH even after 1400 days.

46

6. Conclusions

Simulations of 'end-point' pH measurements in batch bentonite-water slurry experiments showed different pH values according to the complexity of the system studied. The most complete system investigated (clay hydrolysis + cation exchange + trace mineral solubility + clay edge protonation-deprotonation reactions) revealed that pH values were a strong function of partial pressure of carbon dioxide, with pH increasing with decreasing PCO_2 (log PCO_2 values ranging from -3.5 to -7.5 bars produced pH values ranging from 7.9 to 9.6). A slightly less-complex system excluding clay mineral hydrolysis produced essentially identical pH values ranging across the same values of PCO_2. Therefore these 'end-point' calculations showed that the inclusion of clay mineral hydrolysis has an insignificant impact upon calculated pore fluid pH.

A second set of calculations investigated disequilibrium between clay and pore fluid in laboratory squeezing cell tests involving pure water (pH = 9.0) or a 1M NaOH solution (pH = 12.1). For these calculations, the presence of trace minerals, clay cation exchange, and protonation-deprotonation reactions were ignored in the interests of focusing upon the effects of clay hydrolysis. Simulations carried out for 100 days (the same timescale as the experiments) showed that smectite remained far from equilibrium throughout, but pH decreases due to smectite hydrolysis were trivial. These calculations confirmed that on the timescale of the experiments, the effects of clay hydrolysis are insignificant in modifying pore fluid composition. However, extending the duration of the simulations to that required for clay-fluid equilibrium, necessitated timescales of 7 and 65 years for pure water and 1M NaOH, respectively, but produced relatively minor pH decreases in the order of 0.1-0.2 pH units. However, if the (equilibrium) precipitation of secondary minerals was included in the simulations, then not only was the clay-fluid equilibration period extended dramatically (from 7 to 360 years for pure water, and from 65 to 2600 years for 1 M NaOH), but concomitant changes in pH were significant, decreasing from 9.0 to 8.6 (pure water) and from 12.1 to 9.0 (1 M NaOH). Repetition of these latter calculations using an alternative method of estimating the ΔG_f^0 of smectite (Vieillard model replacing the Polymer model) produced an increase in equilibrium time for reaction with 1M NaOH from 2600 to 5000 years, highlighting the potential effects of the uncertainty in thermodynamic data for smectite.

A final set of calculations was carried out to investigate both the time- and space-dependent variations in pore fluid composition in laboratory in-diffusion experiments conducted for over 1200 days, initially with pure water and 'spiked' after 271 days with a Na-Ca-OH-Cl solution (pH = 11.7). These calculations confirmed that smectite hydrolysis alone has an insignificant impact upon pH buffering over lab timescales and that the pH buffering observed is most likely controlled by clay protonation-deprotonation reactions, and kinetic secondary mineral (brucite + tobermorite) precipitation, using a total porosity model (simulations using a geochemical porosity value produced a poor fit to the experimental data). Ion exchange was not important in controlling pH. The pH of the initial bentonite pore water is ascribed

to the presence of trace amounts of CO_2 in the experiments, although calcite played an insignificant role in pH buffering. Alternative data for the kinetic hydrolysis of smectite produced no observable differences, and the adoption of a reduced diffusion coefficient produced a poorer fit to experiment results.

In conclusion, modelling does not support the view that because smectite dissolution is very slow, it is a process of minor importance in the geochemical evolution of the near field. However, the modelling does predict that the effects of smectite dissolution on the chemistry of bentonite pore waters would be essentially undetectable over experimental time scales of a few years at most. When the model is combined with plausible constraints on the precipitation of secondary phases, however, significant changes in solution chemistry and mineralogy are predicted to occur over time scales that are certainly relevant to near-field evolution (hundreds to thousands of years).

There are remaining fundamental uncertainties related to the variable chemistry of the smectite clays, the nature of porosity in highly compacted buffer materials, the reactive surface area of smectite, and the thermodynamic properties of these clay minerals. Studies of natural clay-water systems that have evolved over long periods of time could help provide a new perspective on these uncertainties, and approaches that could be used to help resolve them.

7. References

[1] Nagra (2002) Project Opalinus Clay Safety Report. Demonstration of disposal feasibility for spent fuel, vitrified high-level waste and long-lived intermediate-level waste (Entsorgungsnachweis). Nagra, Wettingen, Switzerland, Nagra Technical Report 02-05.

[2] SKB (2006) Long-term safety for KBS-3 repositories at Forsmark and Laxemar - a first evaluation. Main report of the SR-Can project. Swedish Nuclear Fuel and Waste Management Company, Stockholm, Sweden, SKB Technical Report TR-06-09.

[3] Stumm, W. and Morgan, J.J. (1981) Aquatic Geochemistry, 2nd Edition. New York, USA: Wiley-Interscience.

[4] Arthur, R.C. and Wang, J. (2000) Claystone constraints on models of the long-term chemical evolution of buffer porewaters. Scientific Basis for Nuclear Waste Management (R. W. Smith and D. W. Shoesmith, eds.), vol. 608, pp. 551-556.

[5] Savage, D., Benbow, S., Watson, C., Takase, H., Ono, K., Oda, C., and Honda, A. (2010) Natural systems evidence for the alteration of clay under alkaline conditions: an example from Searles Lake, California. Applied Clay Science, vol. 47, pp. 72-81.

[6] Muurinen, A. and Carlsson, T. (2007) Development of methods for on-line measurements of chemical conditions in compacted bentonite. Physics and Chemistry of the Earth, vol. 32, pp. 241-246.

[7] Kozaki, K., Fujishima, A., Sato, S. and Ohashi, H, (1998) Self-diffusion of sodium ions in compacted sodium montmorillonite. Nuclear Technology, vol. 121, pp. 63-69.

[8] Kozaki, T., Inada, K.A., Sato, S. and Ohashi, H. (2001) Diffusion mechanism of chloride ions in sodium montmorillonite. Journal of Contaminant Hydrology, vol. 47, pp. 159-170.

[9] Bradbury, M.H. and Baeyens, B. (2002) Porewater chemistry in compacted re-saturated MX-bentonite. Physicochemical characterisation and geochemical modelling. Paul Scherrer Institute, Villigen, Switzerland, PSI Report 02-10.

[10] Bradbury, M.H. and Baeyens, B. (2003) Porewater chemistry in compacted re-saturated MX-80 bentonite. Journal of Contaminant Hydrology, vol. 61, pp. 329-338.

[11] Kozaki, T., Fujishima, A., Saito, N., Sato, S. and Ohashi, H. (2005) Effects of dry density and exchangeable cations on the diffusion process of sodium ions in compacted bentonite. Engineering Geology, vol. 81, pp. 246-254.

[12] Glaus, M.A., Baeyens, B., Bradbury, M.H., Jakob, A., Van Loon, L.A. and Yaroshchuck, A. (2007) Diffusion of 22Na and 85Sr in Montmorillonite: Evidence of interlayer diffusion being the dominant pathway at high compaction. Environmental Science and Technology, vol. 41, pp. 478-485.

[13] Muurinen, A., Karnland, O. and Lehikoinen, J. (2004) Ion concentration caused by external solution into the porewater of compacted bentonite. Physics and Chemistry of the Earth, vol. 29, pp. 119-127.

[14] Karnland, O., Muurinen, A. and Karlsson, F. (2002) Bentonite swelling pressure in NaCl solutions - experimentally determined data and model calculations. In Symposium on Large-Scale Field Tests in Granite, Sitges, Spain.

[15] Birgersson, M. and Karnland, O. (2009) Ion equilibrium between montmorillonite interlayer space and an external solution. Geochimica et Cosmochimica Acta, vol. 73, pp. 1908-1923.

[16] Karnland, O., Muurinen, A. and Karlsson, F. (2005) Bentonite swelling pressure in NaCl solutions – Experimentally determined data and model calculations. in Advances in Understanding Engineered Clay Barriers, E. E. Alonso and A. Ledesma, Eds. London, UK: Taylor & Francis Group.

[17] Birgersson, M, Karnland, O. and Nilsson, U. (2008) Freezing in saturated bentonite – A thermodynamic approach. Physics and Chemistry of the Earth, vol. 33, pp. S527-S530.

[18] Karnland, O., Olsson, S., Nilsson, U. and Sellin, P. (2007) Experimentally determined swelling pressures and geochemical interactions of compacted Wyoming bentonite with highly alkaline solutions. Physics and Chemistry of the Earth, vol. 32, pp. 275-286.

[19] Muurinen, A. and Carlsson, T. (2007) Eh and pH in compacted MX-80 bentonite. European Commission, Brussels, Belgium, NF-PRO RTD2 Deliverable 2.2.14.

[20] Arcos, D., Grandia, F. and Domènech, C. (2006) Geochemical evolution of the near field of a KBS-3 repository. Swedish Nuclear Fuel and Waste Management Company, Stockholm, Sweden, SKB Technical Report TR-06-16.

[21] Guillaume, D., Neaman, A., Cathelineau, M., Mosser-Ruck, R., Peiffert, C., Abdelmoula, M., Dubessy, J., Villiéras, F., Baronnet, A. and Michau, N. (2003) Experimental synthesis of chlorite from smectite at 300 °C in the presence of metallic Fe. Clay Minerals, vol. 38, pp. 281-302.

[22] Vieillard, P. (2000) A new method for the prediction of Gibbs free energies of formation of hydrated clay minerals based on the electronegativity scale. Clays and Clay Minerals, vol. 48, pp. 459–473.

[23] Mattigod, S.V. and Sposito, G. (1978) Improved method for estimating the standard free energies of formation ($\Delta G0f,298.15$) of smectites. Geochimica et Cosmochimica Acta, vol. 42, pp. 1753-1762.

[24] Vieillard, P. (2002) A new method for the prediction of Gibbs free energies of phylosilicates, 10 angstroms and 14 angstroms based on the electronegativity scale. Clays and Clay Minerals, vol. 50, pp. 352–363.

[25] Johnson, J.W., Oelkers, E.H., and Helgeson, H.C. (1992) SUPCRT92. A software package for calculating the standard molal thermodynamic properties of minerals, gases, aqueous species, and reactions from 1 to 5000 bar and 0 to 1000 °C. Computers and Geoscience, vol. 18, pp. 899-947.

[26] Sposito, G. (1986) The polymer model of thermochemical clay mineral stability," Clays and Clay Minerals, vol. 34, pp. 198-203.

[27] Bethke, C.M. (2008) Geochemical and Biogeochemical Reaction Modeling. Cambridge, UK: Cambridge University Press.

[28] Wilkin, R.T. and Barnes, H.L. (1998) Solubility and stability of zeolites in aqueous solution: I. Analcime, Na-, and K-clinoptilolite. American Mineralogist, vol. 83, pp. 746-761.

[29] Chipera, S.J. and Apps, J.A. (2001) Geochemical stability of natural zeolites, in Natural Zeolites: Occurrence, Properties, Applications. vol. 45, D. L. Bish and D. W. Ming, Eds. Blacksburg, Virginia, USA: Mineralogical Society of America, pp. 117-161.

[30] Sato, T., Kuroda, M., Yokoyama, S., Tsutsui, M., Fukushi, K., Tanaka, T. and Nakayama, S. (2004) Dissolution mechanism and kinetics of smectite under alkaline conditions. In International Workshop on Bentonite-Cement Interaction in Repository Environments, Tokyo, Japan.

[31] Rozalén, M.L., Huertas, F.J., Brady, P.V., Cama, J., García-Palma, S. and Linares, J. (2008) Experimental study of the effect of pH on the kinetics of montmorillonite dissolution at 25 °C. Geochimica et Cosmochimica Acta, vol. 72, pp. 4224-4253.

[32] Tsutsui, M., Kuroda, M., Yokoyama, S., Pascua, C., Ringor, C., and Sato, T. (2005) Reactive surface area in smectite dissolution under highly alkaline condition. In Clays in Natural and Engineered Barriers for Radioactive Waste Confinement, Tours, France, pp. 335-336.

[33] Tournassat, C., Neaman, A., Villiéras, F., Bosbach, D. and Charlet, L. (2003) Nanomorphology of montmorillonite particles: estimation of the clay edge sorption site density by low-pressure gas adsorption and AFM observations. American Mineralogist, vol. 88, pp. 1989-1995.

[34] D. Savage, C. Walker, R. C. Arthur, C. A. Rochelle, C. Oda, and H. Takase, "Alteration of bentonite by hyperalkaline fluids: a review of the role of secondary minerals," Physics and Chemistry of the Earth, vol. 32, pp. 287-297, 2007.

[35] Palandri, J.L. and Kharaka, Y.K. (2004) A compilation of rate parameters of water-mineral interaction kinetics for application to geochemical modelling," United States Geological Survey, Menlo Park, California, USA, USGS Open File Report 2004-1068.

[36] Busenberg, E. and Plummer, L.N. (1986) A comparative study of the dissolution and crystal growth kinetics of calcite and aragonite. F. A. Mumpton, Ed.: U.S. Geological Survey, pp. 139-168.

[37] Plettinck, S., Chou, L. andWollast, R. (1994) Kinetics and mechanisms of dissolution of silica at room temperature and pressure. Mineralogical Magazine, V.M. Goldschmidt Abstracts, vol. 58A, pp. 728-729.

[38] Savage, D., Rochelle, C.A., Moore, Y., Milodowski, A., Bateman, K., Bailey, D. and Mihara, M. (2001) Analcime reactions at 25-90 °C in hyperalkaline fluids. Mineralogical Magazine, vol. 65, pp. 571-587.

[39] Parkhurst, D.L. and Appelo, C.A.J. (1999) User's guide to PHREEQC (Version 2) - a computer program for speciation, batch-reaction, one-dimensional transport, and inverse geochemical calculations," U.S. Geological Survey U.S. Geological Survey Water-Resources Investigations Report 99-4259.

[40]   Quintessa (2010) QPAC: Quintessa's General-Purpose Modelling
        Code," Quintessa Limited, Henley-on-Thames, UK, Quintessa Re-
        port QRS-QPAC-11 v1.0.